Atmos. Chem. Phys. Discuss., 15, 30321–30381, 2015
www.atmos-chem-phys-discuss.net/15/30321/2015/
doi:10.5194/acpd-15-30321-2015

Atmospheric Chemistry and Physics Discussions

Theoretical analysis of mixing in liquid clouds – Part 3: Inhomogeneous mixing

M. Pinsky[1], **A. Khain**[1], **and A. Korolev**[2]

[1]Department of Atmospheric Sciences, The Hebrew University of Jerusalem, Jerusalem, Israel
[2]Environment Canada, Cloud Physics and Severe Weather Section, Toronto, Canada

Received: 26 August 2015 – Accepted: 5 October 2015 – Published: 4 November 2015

Correspondence to: A. Khain (khain@vms.huji.ac.il)

Published by Copernicus Publications on behalf of the European Geosciences Union.

Abstract

An idealized model of time-dependent mixing between cloud and non-cloud volumes is analyzed. Initial droplet size distribution (DSD) in cloud volume is assumed to be monodisperse. Both analytical investigation and parcel model investigation are used to study mixing processes and solve diffusion-evaporation equations.

It is shown that the evolution of microphysical variables and the final equilibrium stage are unambiguously determined by two non-dimensional parameters. The first parameter, R, which is proportional to the ratio of the saturation deficit to the liquid water content in a cloud volume, determines whether the equilibrium stage is reached at 100 % relative humidity, or, rather, leads to a full evaporation of cloud droplets. The second parameter, Da, is the Damkölher number, which is equal to the ratio of the characteristic mixing time and phase relaxation time. This parameter (together with parameter R) determines whether mixing takes place according to a homogeneous or an inhomogeneous scenario.

An analysis of the results obtained within a wide range of parameters R and Da is presented. It is shown that there is no pure homogeneous mixing, since the first stage of mixing is always inhomogeneous. Turbulent mixing between different volumes always starts as inhomogeneous and the mixing type can change during the mixing process. At any values of governing parameters, mixing leads to the formation of a tail of small droplets in the DSD and therefore to DSD broadening. The broadening depends on Da and the final DSD dispersion can be as large as 0.2 at large Da. The total duration of the mixing process varies from several to one hundred phase relaxation times, depending on R and Da. Delimitation between the types of mixing on the Da–R plane is carried out. The definitions of homogeneous and inhomogeneous mixings are reconsidered and clarified. The paper also compares the results of the current study with those obtained with classical mixing concepts.

ACPD
15, 30321–30381, 2015

1 Introduction

Cloud physics literature typically considers two types of turbulent mixing: homogeneous and inhomogeneous (e.g. Burner and Brenguier, 2006; Devenish et al., 2012; Kumar et al., 2012). The concept of inhomogeneous mixing in clouds was introduced by Baker and Latham (1979), Baker et al. (1980) and Blyth et al. (1980). In a laboratory experiments by Latham and Reed (1977) showed that mixing of cloud environment and sub-saturated air resulted in complete evaporation of some droplets, whereas others remained unchanged. The detailed analysis of classical concepts of homogeneous and inhomogeneous mixing is given in the study by Korolev et al. (2015, hereafter Pt1).

The studies of inhomogeneous mixing were closely related to exploration of different mechanisms explaining enhanced growth of cloud droplets and warm precipitation formation (Baker et al., 1980; Baker and Latham, 1982). However, the concepts of homogeneous and inhomogeneous mixing have a much wider application in cloud physics than simply the formation of large-sized droplets assumed in cases of extreme inhomogeneous mixing. In fact, they are closely related to mechanisms involved in the formation of DSDs in clouds and to the description of such formations in numerical cloud models. Pinsky et al. (2015) (hereafter referred to as Pt2) discussed the mechanisms of homogeneous mixing. It was shown that homogeneous mixing takes place at scales below about 0.5 m. In air volumes of larger scales, droplets located in different parts of the volume experience different subsaturations (saturation deficits). Such mixing is considered to be inhomogeneous. In addition to the terms "homogeneous" and "inhomogeneous" mixing, many studies also used the term "extreme inhomogeneous" mixing (see Pt1). In this study, we propose quantitative delimitation of the mixing types.

According to a widely accepted classical conceptual scheme, extreme inhomogeneous mixing consists of two main stages. During the first stage some fraction of droplets is transported into the dry entrained volume and completely evaporates. This process continues until the evaporating droplets saturate the volume. At the second stage, turbulent mixing between the cloud volume and the droplet-free saturated vol-

ACPD
15, 30321–30381, 2015

ume homogenizes the gradients of the droplet concentration and other quantities. Since both volumes are saturated, mixing does not affect droplet sizes. As a result, the final (equilibrium) stage is characterized by relative humidity RH = 100 % and the DSD having the shape similar to that before mixing, but with a lower droplet concentration. The same result (decrease in droplet concentration but unchanged droplet size) is expected in cases of both monodisperse and polydisperse DSDs. Since the shape of the DSD does not change, the characteristic droplet sizes (i.e. mean square, mean volume, effective radii) also do not change in the course of inhomogeneous mixing (see Pt1).

Strictly speaking, according to the classical concepts, the final equilibrium state with RH = 100 % is reached either by the partial evaporation of all droplets (homogeneous mixing) or the total evaporation of a certain portion of droplets without affecting the remaining droplets (inhomogeneous mixing) (Lehmann et al., 2009; Pt1).

It was hypothesized that decrease of the droplet concentration during entrainments and mixing may promote enhanced growth of large cloud droplets and facilitate the early formation of raindrops in convective clouds (Telford and Chai, 1981; Baker and Latham, 1982). This hypothesis is based on the assumption that after mixing during the following ascent the same amount of adiabatically condensed water will be shared between smaller number of droplets (than without mixing), and the smaller number of droplets will grow to a larger sizes.

Since the early works of Warner (1969), Baker and Latham (1979) numerous observational and numerical studies dedicated to the effects of entrainment and mixing on DSD formation have been carried out. Most the theoretical studies were focused on the final stage of mixing. In analyses of in-situ measurements, the observed data were compared with those expected at the final stage of mixing. If the droplet concentration decreases without a corresponding change in the characteristic droplet radius, such mixing is deemed "extremely inhomogeneous." In contrast, if the characteristic droplet radius decreases with an increase of the dilution level, the droplet concentration change is insignificant and the mixing was identified as "homogeneous." In cases

ACPD
15, 30321–30381, 2015

when both the characteristic droplet radius and the droplet concentration change, the mixing was considered as "intermediate". The microphysical processes that describe intermediate mixing remain largely uncertain.

It is clear that the application of the concepts of homogeneous and inhomogeneous mixing depends on the spatial scale of mixing volumes (Pt1). In the frame of existing convention the mixing is considered as homogeneous if $\tau_{mix}/\tau_{pr} \ll 1$, where $\tau_{mix} \sim L^{2/3}\varepsilon^{-1/3}$ is the characteristic time scale of turbulent mixing of a volume with a characteristic linear scale L of an entrained volume, and $\tau_{pr} = \left(4\pi D\overline{r}N\right)^{-1}$ is time of phase relaxation, characterizing response of the population of droplets to the changes of humidity. Here ε is dissipation rate of turbulent kinetic energy, N is a concentration of droplets in cloud volume, $\overline{r}$ is a mean radius of droplets and D is the diffusivity of water vapor (a list of notations of variables used in the study is given in Table A1). In this case, the process of homogeneous mixing can be divided into two stages. During the first stage, the initial gradients of microphysical and thermodynamic variables rapidly decrease to zero. By the end of this stage the temperature, humidity (hence, supersaturation) and droplet concentration fields are spatially homogenized. During the second stage, which duration is relatively long, droplets evaporate and increase the relative humidity in the volume. The process ends when the relative humidity (RH) becomes equal to 100 %, or when all droplets completely evaporate, so that the final RH $\leq$ 100 %. At scales larger than $\sim$ 0.5 m, $\tau_{mix}/\tau_{pr} > 1$ and the spatial gradients of RH remain for a long time. Consequently, droplets within mixing volumes experience different subsaturations and the mixing should be considered as inhomogeneous. If $\tau_{mix}/\tau_{pr} \gg 1$, the mixing is considered to be extremely inhomogeneous.

In this study, we analyze the process of inhomogeneous mixing in cases when the initial DSD in a cloud volume is monodisperse. The structure of the paper is as follows. The main concept and the basic equations for time-dependent inhomogeneous mixing are described in Sect. 2. An analysis of non-dimensional diffusion-evaporation equations is presented in Sect. 3. The design and results of simulations of non-homogeneous mixing are obtained in Sects. 4 and 5. A discussion clarifying

ACPD
15, 30321–30381, 2015

the concepts of homogeneous and inhomogeneous mixing is presented in concluding Sect. 6. The results obtained in the present study are reduced in the limiting case of $\tau_{mix}/\tau_{pr} \to 0$ to those obtained in Pinsky et al. (2015, hereafter, Pt2).

2 Main concept and the basic equations

During mixing of cloud and entrained volumes the following two processes determine changing of microphysical and thermodynamical variables: first is the turbulent diffusion resulting in mechanical stirring the environment and smoothening the gradients of temperature, water vapor and droplet concentration, whereas the second process is related to the reaction of the population of droplets on the undersaturated environment resulting in droplet evaporation and phase transformation. In the frame of this study the process of inhomogeneous mixing is investigated basing on the analysis and solution of 1-D diffusion-evaporation equation. The conceptual cartoon presenting initial conditions used in the following discussion is shown in Fig. 1.

Let us consider mixing of two equal volumes: the cloud volume (left in Fig. 1) and the dry volume (right in Fig. 1), each has a linear size of $L/2$. The value of L is thought to be the external turbulence scale, of several tens or a few hundred meters. The mixing starts at $t = 0$. The process of mixing of two volumes is considered to be adiabatic: i.e. at the domain of mixing the mass and energy are conserved. The cloud volume is initially saturated $S_1 = 0$, the initial droplet concentration is N_1, and the initial liquid water mixing ratio is $q_{w1} = \frac{4\pi\rho_w}{3\rho_a} N_1 r_0^3$. In the cloud-free (right) volume at the initial moment $RH_2 < 100\,\%$ (i.e. $S_2 < 0$), $N_2 = 0$, and $q_{w2} = 0$. Therefore, the initial profiles of these quantities along the x axis are step functions

$$N(x,0) = \begin{cases} N_1 & \text{if } 0 \le x < L/2 \\ 0 & \text{if } L/2 \le x < L \end{cases} \qquad (1a)$$

ACPD
15, 30321–30381, 2015

$$S(x,0) = \begin{cases} 0 & \text{if } 0 \le x < L/2 \\ S_2 & \text{if } L/2 \le x < L \end{cases} \quad (1b)$$

$$q_w(x,0) = \begin{cases} q_{w1} & \text{if } 0 \le x < L/2 \\ 0 & \text{if } L/2 \le x < L \end{cases} \quad (1c)$$

The initial profile of droplet concentration is shown in Fig. 1. This is the simplest inhomogeneous mixing scheme, wherein mixing takes place only in the direction x, and the vertical velocity is neglected. The process of turbulent diffusion (turbulent mixing) is described by a 1-D equation of turbulent diffusion with a turbulent coefficient K. The mixing is assumed to be driven by isotropic turbulence within the inertial sub-range, where Richardson's law is valid. In this case, turbulent coefficient is evaluated as in Monin and Yaglom (1975)

$$K(L) = C\varepsilon^{1/3}L^{4/3} \quad (2)$$

In Eq. (2) C is a constant. Equation (2) means that turbulent diffusion occurs at scales much larger than the Kolmogorov microscale, i.e. at scales where processes of molecular diffusion can be neglected.

Since the total volume is adiabatic, the fluxes of different quantities through the left and right boundaries at any time instance are equal to zero, i.e.

$$\frac{\partial N(0,t)}{\partial x} = \frac{\partial N(L,t)}{\partial x} = 0; \quad \frac{\partial q_w(0,t)}{\partial x} = \frac{\partial q_w(L,t)}{\partial x} = 0; \quad \frac{\partial q_v(0,t)}{\partial x} = \frac{\partial q_v(L,t)}{\partial x} = 0 \quad (3)$$

where q_v is the water vapor mixing ratio.

Since during mixing different droplets experience different supersaturations, the initially monodisperse DSD will turn into polydisperse DSD. The droplets that were transported into an initially dry volume will undergo either partial or complete evaporation. This evaporation leads to a decrease in both droplet size and droplet concentration.

ACPD
15, 30321–30381, 2015

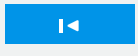

Now we will derive the basic system of equation that describes the processes of diffusion and evaporation which occur simultaneously. The first equation is written for value Γ defined as

$$\Gamma = S + A_2 q_w \tag{4}$$

This value is conservative in a moist adiabatic process, i.e. its value is insensitive to phase transitions (Pinsky et al., 2013, 2014). In Eq. (4) the coefficient $A_2 = \frac{1}{q_v} + \frac{L_w^2}{c_p R_v T^2}$ is weak function of temperature, and it changes by ∼ 10 % when temperatures change by ∼ 10 °C (Pinsky et al., 2013). In this study, it is assumed that A_2 = constant. In Eq. (4) $q_w = \frac{4\pi\rho_w}{3\rho_a} \int_0^\infty r^3 g(r) Dr$) is the liquid water mixing ratio and $g(r)$ is the DSD. The quantity Γ obeys the diffusion equation

$$\frac{\partial \Gamma(x,t)}{\partial t} = K \frac{\partial^2 \Gamma(x,t)}{\partial x^2} \tag{5}$$

with the boundary conditions $\frac{\partial \Gamma(0,t)}{\partial x} = \frac{\partial \Gamma(L,t)}{\partial x} = 0$ and the initial profile at $t = 0$

$$\Gamma(x,0) = \begin{cases} A_2 q_{w1} & \text{if } 0 \le x < L/2 \\ S_2 & \text{if } L/2 \le x < L \end{cases} \tag{6}$$

Therefore, in the left volume, function $\Gamma(x,0)$ is positive, and in the right volume it is negative.

Since Γ does not depend on phase transitions, Eq. (5) can be solved independently of other equations. The solution of Eq. (5) with initial condition Eq. (6) is (Polyanin and Zaitsev, 2004)

$$\Gamma(x,t) = \sum_{n=0}^{\infty} a_n \exp\left(-\frac{K n^2 \pi^2 t}{L^2}\right) \cos\left(\frac{n\pi x}{L}\right) = \tag{7}$$

ACPD
15, 30321–30381, 2015

$$\frac{1}{2}(S_2 + A_2 q_{w1}) + (A_2 q_{w1} - S_2) \sum_{n=1}^{\infty} \frac{\sin(n\pi/2)}{n\pi/2} \exp\left(-\frac{K n^2 \pi^2 t}{L^2}\right) \cos\left(\frac{n\pi x}{L}\right)$$

where the Fourier coefficients of expanding the step function Eq. (6) are

$$a_0 = \frac{1}{2}(A_2 q_{w1} + S_2) \tag{8a}$$

$$a_n = (A_2 q_{w1} - S_2) \frac{\sin(n\pi/2)}{n\pi/2}, n = 1, 2, \ldots \tag{8b}$$

An example of the spatial dependencies of $\Gamma(x,t)$ at different time instances during the mixing is shown in Fig. 2. One can see a decrease in the initial gradients and a tendency to establish a horizontally uniform value of Γ. Since the initial volume was divided into two equal parts, the diffusion leads to a formation of the constant limit value of function Γ

$$\Gamma(x,\infty) = \frac{1}{2}(\Gamma(0,0) + \Gamma(L,0)).$$

The second basic equation is the equation for diffusional droplet growth taken in the following form (Pruppacher and Klett, 2007)

$$\frac{d\sigma}{dt} = \frac{2S}{F} \tag{9}$$

where $\sigma = r^2$ is the square radius of droplets and $F = \frac{\rho_w L_w^2}{k_a R_v T^2} + \frac{\rho_w R_v T}{e_w(T) D}$. The value of the coefficient F is considered as constant in this study. The solution to Eq. (9) is

$$\sigma(t) = \frac{2}{F} \int_0^t S(t')dt' + \sigma_0 \tag{10}$$

ACPD
15, 30321–30381, 2015

The third main equation describes the evolution of DSD. In the following discussion the DSD will be described in a form $f(\sigma)$, which is the distribution of the square of the radius. Such presentation directly utilizes the property of the diffusion growth Eq. (9) according to which changes made to the square radius during DSD evolution do not depend on the drop radius. The time changes of DSD are reduced to shifting distributions, while the shape of the distribution is assumed to remain the same. The standard DSD $g(r)$ is related to $f(\sigma)$ as $g(r) = 2r \cdot f(\sigma)$.

The normalized condition for $f(\sigma)$ is

$$N = \int_0^\infty f(\sigma)\mathrm{d}\sigma \tag{11}$$

where N is the droplet concentration. Using DSD $f(\sigma)$, the liquid water mixing ratio can be represented as integral

$$q_\mathrm{w} = \frac{4\pi\rho_\mathrm{w}}{3\rho_\mathrm{a}} \int_0^\infty \sigma^{3/2} f(\sigma)\mathrm{d}\sigma \tag{12}$$

The 1-D diffusion-evaporation equation for non-conservative function $f(\sigma)$ can be written in the form (Rogers and Yau, 1989)

$$\frac{\partial f(\sigma)}{\partial t} = K\frac{\partial^2 f(\sigma)}{\partial x^2} + \frac{\partial}{\partial \sigma}\left(\frac{\mathrm{d}\sigma}{\mathrm{d}t} f(\sigma)\right) \tag{13}$$

where the first term on the right-hand side of Eq. (13) describes changes in the DSD due to the process of spatial diffusion, while the second term on the right-hand side describes changes in the DSD due to evaporation. Substitution of Eq. (9) into Eq. (13) leads to

$$\frac{\partial f(x,t,\sigma)}{\partial t} = K\frac{\partial^2 f(x,t,\sigma)}{\partial x^2} + \frac{2S(x,t)}{F}\frac{\partial f(x,t,\sigma)}{\partial \sigma} \tag{14}$$

ACPD
15, 30321–30381, 2015

To close Eq. (14) one should use conservative Eq. (4) in the form

$$S(x,t) = \Gamma(x,t) - A_2 q_w(x,t) \tag{15}$$

where $q_w(x,t)$ is calculated according to Eq. (12). Equations (12), (14), and (15) represent a closed set of equations allowing the calculation of $f(x,t,\sigma)$.

It is interesting to consider equations for moments of DSD. Let us define a moment of DSD $f(\sigma)$ of order α as

$$m_\alpha = \overline{\sigma^\alpha} = \int_0^\infty \sigma^\alpha f(\sigma) \mathrm{d}\sigma \tag{16}$$

Multiplying Eq. (14) by σ^α, integrating within limits $[0,\ldots,\infty]$ and assuming that $\sigma^\alpha f(\sigma) \to 0$ when $\sigma \to \infty$ yield a recurrent formula for DSD moments

$$\frac{\partial m_\alpha(x,t)}{\partial t} = K \frac{\partial^2 m_\alpha(x,t)}{\partial x^2} - \alpha \frac{2S}{F} m_{\alpha-1}(x,t) \tag{17}$$

Equation (17) provides a recurrent relationship between moments of different orders. Such a relationship was discussed in Pinsky et al.'s (2014) analysis of diffusion growth in an ascending adiabatic parcel.

In particular, the equation for liquid water mixing ratio that is a moment of the order of $\alpha = \frac{3}{2}$ can be written as

$$\frac{\partial q_w(x,t)}{\partial t} = K \frac{\partial^2 q_w(x,t)}{\partial x^2} - \frac{4\pi\rho_w N(x,t)\overline{r}(x,t)}{F\rho_a} S(x,t) \tag{18}$$

where the mean radius $\overline{r}(x,t) = \frac{m_{1/2}}{m_0}$.

In the general case Eq. (18) is not closed, since concentration $N(x,t)$, and $\overline{r}(x,t)$ are unknown functions of the time and spatial coordinates.

ACPD
15, 30321–30381, 2015

The characteristic time of the process of evaporation and the change in supersaturation is the phase relaxation time (Korolev and Mazin, 2003; Pt1)

$$\tau_{\mathrm{pr}} = \frac{\rho_{\mathrm{a}} F}{4\pi\rho_{\mathrm{w}} A_2 N \bar{r}} \tag{19}$$

Using Eq. (19), Eq. (18) can be rewritten as

$$\frac{\partial q_{\mathrm{w}}(x,t)}{\partial t} = K\frac{\partial^2 q_{\mathrm{w}}(x,t)}{\partial x^2} - \frac{1}{\tau_{\mathrm{pr}}(x,t)}\left[\frac{1}{A_2}\Gamma(x,t) - q_{\mathrm{w}}(x,t)\right] \tag{20}$$

$$= K\frac{\partial^2 q_{\mathrm{w}}(x,t)}{\partial x^2} - \frac{1}{A_2\tau_{\mathrm{pr}}(x,t)}S(x,t)$$

From Eqs. (20) and (15), the equation for supersaturation can be written in the following simple form

$$\frac{\partial S(x,t)}{\partial t} = K\frac{\partial^2 S(x,t)}{\partial x^2} + \frac{S(x,t)}{\tau_{\mathrm{pr}}(x,t)} \tag{20a}$$

Equations (20) and (20a) show that changes in microphysical variables are determined by the rate of spatial diffusion (the first term on the right-hand side of these equations) and evaporation (the second term on the right-hand side). Equation similar to Eq. (20a) was used by Jeffery and Reisner (2006).

3 Analysis of non-dimensional equations

Spatial diffusion and evaporation depend on many parameters. An analysis best begins with the basic equation system sketched out in non-dimensional form. Let us define a time scale corresponding to the initial phase relaxation time in a cloud volume

$$\tau_{01} = \tau_0 = \frac{\rho_{\mathrm{a}} F}{4\pi\rho_{\mathrm{w}} A_2 N_1 r_0} \tag{21}$$

ACPD
15, 30321–30381, 2015

and non-dimensional time $\widetilde{t} = t/\tau_0$. We also use the following non-dimensional parameters:

Non-dimensional phase relaxation time

$$\widetilde{\tau}_{\mathrm{pr}} = \tau_{\mathrm{pr}}/\tau_0 = \frac{N_1 r_0}{N(\widetilde{x},\widetilde{t})\overline{r}(\widetilde{x},\widetilde{t})}, \tag{22a}$$

normalized liquid water mixing ratio

$$\widetilde{q} = \frac{q_{\mathrm{w}}}{q_{\mathrm{w1}}}, \tag{22b}$$

normalized supersaturation

$$\widetilde{S} = \frac{S}{A_2 q_{\mathrm{w1}}}, \tag{22c}$$

non-dimensional conservative function

$$\widetilde{\Gamma} = \frac{\Gamma}{A_2 q_{\mathrm{w1}}}, \tag{22d}$$

normalized square of droplet radius

$$\widetilde{\sigma} = \frac{\sigma}{r_0^2}, \tag{22e}$$

normalized droplet concentration

$$\widetilde{N} = N/N_1 \tag{22f}$$

and non-dimensional DSD

$$\widetilde{f}(\widetilde{\sigma}) = \frac{r_0^2}{N_1} f(\sigma). \tag{22g}$$

ACPD
15, 30321–30381, 2015

The definition Eq. (22g) means that the integral of a non-dimensional initial size distribution over the normalized square radius is equal to unity.

Non-dimensional distance and non-dimensional time are defined as

$$\widetilde{x} = x/L; \quad \widetilde{t} = t/\tau_0 \tag{22h}$$

The most widely used non-dimensional parameter showing comparative rates of diffusion and evaporation is the Damkölher number:

$$Da = \frac{\tau_{\text{mix}}}{\tau_0} = \frac{L^2}{K\tau_0} \tag{23}$$

where

$$\tau_{\text{mix}} = \frac{L^2}{K} \tag{24}$$

is characteristic time of mixing.

Using these non-dimensional parameters, Eq. (20) can be rewritten in non-dimensional form

$$\frac{\partial \widetilde{q}(\widetilde{x},\widetilde{t})}{\partial \widetilde{t}} = \frac{1}{Da}\frac{\partial^2 \widetilde{q}(\widetilde{x},\widetilde{t})}{\partial \widetilde{x}^2} - \frac{1}{\widetilde{\tau}_{\text{pr}}(\widetilde{x},\widetilde{t})}\left[\widetilde{\Gamma}(\widetilde{x},\widetilde{t}) - \widetilde{q}(\widetilde{x},\widetilde{t})\right] \tag{25}$$

$$= \frac{1}{Da}\frac{\partial^2 \widetilde{q}(\widetilde{x},\widetilde{t})}{\partial \widetilde{x}^2} - \frac{1}{\widetilde{\tau}_{\text{pr}}(\widetilde{x},\widetilde{t})}\widetilde{S}(\widetilde{x},\widetilde{t})$$

where

$$\widetilde{q}(\widetilde{x},\widetilde{t}) = \frac{N(\widetilde{x},\widetilde{t})\overline{\sigma^{3/2}}}{N_1 r_0^3} = \int_0^\infty \widetilde{\sigma}^{3/2}\widetilde{f}(\widetilde{x},\widetilde{t},\widetilde{\sigma})D\widetilde{\sigma} \tag{26}$$

ACPD
15, 30321–30381, 2015

The initial and boundary conditions should be re-written in non-dimensional form as well. For instance, the normalized initial condition for the non-dimensional function $\widetilde{q}(\widetilde{x},0)$ can be derived from Eqs. (1c) and (22b)

$$\widetilde{q}(\widetilde{x},0) = \begin{cases} 1 & \text{if } 0 \le \widetilde{x} < 1/2 \\ 0 & \text{if } 1/2 \le \widetilde{x} < 1 \end{cases} \tag{27}$$

The solution for $\widetilde{\Gamma}(\widetilde{x},\widetilde{t})$ can be obtained by a normalization of solution Eq. (7)

$$\widetilde{\Gamma}(\widetilde{x},\widetilde{t}) = \frac{1}{2}(1+R) + (1-R)\sum_{n=1}^{\infty}\frac{\sin(n\pi/2)}{n\pi/2}\exp\left(-\frac{n^2\pi^2\widetilde{t}}{Da}\right)\cos\left(n\pi\widetilde{x}\right), \tag{28}$$

where

$$R = \frac{S_2}{A_2 q_{w1}} \tag{29}$$

is a non-dimensional parameter. The solution Eq. (28) at $t \to \infty$ depends only on this parameter R

$$\widetilde{\Gamma}(\widetilde{x},\infty) = \frac{1}{2}(1+R) \tag{30}$$

Non-dimensional parameter R is one of the important parameters that controls the process of mixing. In this study, we consider cases when $R < 0$ since $S_2 < 0$, i.e. droplets can only evaporate in the course of mixing. The R yields the ratio of the amount of water vapour that need to be evaporated in order to saturate the mixing environment (that is determined by S_2) and the initial liquid water mixing ratio q_{w1}.

The type of mixing and its result depend on the relationship between the magnitudes of two terms: diffusion and evaporation. The solution of Eq. (25) and the type of mixing depends on the values of two non-dimensional parameters, namely, Da and R. Thus,

ACPD
15, 30321–30381, 2015

if $R = \frac{S_2}{A_2 q_{w1}} < -1$ then $\widetilde{\Gamma}(\widetilde{x}, \infty) < 0$. It means that the droplet-free volume V_2 is too dry and all droplets completely evaporate. At the final equilibrium stage RH < 100 %, i.e. $S(x, \infty) < 0$. If $R = \frac{S_2}{A_2 q_{w1}} > -1$, then $\widetilde{\Gamma}(\widetilde{x}, \infty) > 0$. This means that the mixed volume in the final stage contains droplets, i.e. the mixing leads to an increase in cloud volume. At the final equilibrium stage, RH = 100 % (i.e. $S(x, \infty) = 0$). The case $|R| = \left|\frac{S_2}{A_2 q_{w1}}\right| = \left|\widetilde{S}_2\right| \ll 1$ corresponds to either RH ≈ 100 % (i.e. $S_2 \approx 0$) and/or the liquid water content in the cloud volume is large. In this case, the second term on the right-hand side of Eq. (25) is much smaller than the first term. In this case results of mixing will be driven by the turbulent diffusion only.

The value of *Da* plays the most critical role, since it determines mixing type. In the case $Da \to 0$ (often referred to as homogeneous mixing), the diffusion term at the beginning of the mixing process is much larger than the evaporation (second) term on the right-hand side of Eq. (25). Then, within a short period, the total homogenization of all variables in the mixing volume takes place and all spatial gradients become equal to zero. At this point, the first term on the right-hand side becomes equal to zero, and the second term on the right-hand side of Eq. (25), describing droplet evaporation, becomes dominant. Thus, the process of mixing consists of two stages: a short stage of inhomogeneous mixing and a longer stage of homogeneous mixing. The evolution of the microphysical variables at the stage of homogeneous mixing is described in detail in Pt2.

The case $Da \to \infty$ corresponds to the extremely inhomogeneous mixing, according to the conventional view. In this case the diffusion term is much smaller than the evaporation term, so microphysical processes take place under significant spatial gradients of RH. In the limit of $Da = \infty$ the adjacent volumes do not mix at all, and remain isolated one from another. This case is equivalent to the existence of two independent adiabatic volumes. Another interpretation of the limiting case $Da = \infty$ is an infinite fast droplet evaporation. Both conditions indicate simplifications in the definition of the extremely inhomogeneous mixing as the case when $Da \to \infty$. At intermediate values of

ACPD
15, 30321–30381, 2015

Da the mixing is inhomogeneous, but both factors, turbulent diffusion and evaporation, contribute simultaneously to the formation of the DSD.

Using Eq. (14) and normalization Eq. (22f), the equations for non-dimensional size distribution can be written as

$$\frac{\partial \widetilde{f}(\widetilde{x},\widetilde{t},\widetilde{\sigma})}{\partial \widetilde{t}} = \frac{1}{Da}\frac{\partial^2 \widetilde{f}(\widetilde{x},\widetilde{t},\widetilde{\sigma})}{\partial \widetilde{x}^2} + \frac{2}{3}\left[\widetilde{\Gamma}(\widetilde{x},\widetilde{t}) - \widetilde{q}(\widetilde{x},\widetilde{t})\right]\frac{\partial \widetilde{f}(\widetilde{x},\widetilde{t},\widetilde{\sigma})}{\partial \widetilde{\sigma}} \tag{31}$$

Equation (31) is solved with initial conditions

$$\widetilde{f}(\widetilde{x},0,\widetilde{\sigma}) = \begin{cases} \delta(\widetilde{\sigma}-1) & \text{if } 0 \le \widetilde{x} < 1/2 \\ 0 & \text{if } 1/2 \le \widetilde{x} \le 1 \end{cases} \tag{32}$$

where $\delta(\widetilde{\sigma}-1)$ is a delta function.

Table 1 presents a summary of the non-dimensional variables used in this study and the range of their changes. It is shown that six parameters determining the geometrical and microphysical properties of mixing can be reduced to two non-dimensional parameters. Such representation allows for a more efficient analysis of the mixing process. The ranges of the changes of the variables in Table 1 correspond to the simplifications used in the study: the initial DSD is monodisperse and RH $\le$ 100 %.

4 Design of simulations

4.1 Damkölher number *Da* in clouds

The characteristic mixing time τ_{mix} can be evaluated using Eqs. (2) and (24)

$$\tau_{mix} = \frac{1}{C}\varepsilon^{-1/3}L^{2/3} \tag{33}$$

There is significant uncertainty regarding the evaluation of τ_{mix} and *Da* in clouds. This uncertainty is largely related to the choice of the coefficient *C* in the expression Eq. (33).

ACPD
15, 30321–30381, 2015

In a study by Jeffrey and Reisner (2006), $C = 10$; Lehmann et al. (2009) use $C = 1$. According to Monin and Yaglom (1975) and Boffetta and Sokolov (2002), $C \approx 0.2$.

According to Lehmann et al. (2009), the values of Da in clouds of different types range from to 0.1 to several hundred. Thus, estimation of Da in cloud may vary in a wide range reaching few orders of magnitude. It is interesting that the values of Da in stratocumulus clouds can be similar or even higher than those in cumulus clouds, since both τ_{mix} and τ_{pr} in stratiform clouds are larger than in cumulus clouds.

In our simulations, we compare the evolution of microphysical parameters within a wide range of Da (from 1 up to 500) and R (from −1.5 up to −0.1). $Da = 1$ is considered the case closest to homogeneous mixing, while $Da = 500$ represents extremely inhomogeneous mixing.

4.2 Numerical method

Calculations were performed using MATLAB solver PDEPE. We solve the equation system Eq. (31) for normalized DSD $\widetilde{f}(\widetilde{x},\widetilde{t},\widetilde{\sigma}_j)$ with initial condition Eq. (32) and Neumann boundary conditions

$$\frac{\partial \widetilde{f}(0,\widetilde{t},\widetilde{\sigma}_j)}{\partial \widetilde{x}} = \frac{\partial \widetilde{f}(1,\widetilde{t},\widetilde{\sigma}_j)}{\partial \widetilde{x}} = 0 \tag{34}$$

where $j = 1,\ldots,24$ are the bin numbers on a linear grid of square radii. The number of grid points along the $\widetilde{x}$ axis was set equal to 81.

In calculation of the last term on the right-hand side of Eq. (31), the normalized supersaturation $\widetilde{S}$ was calculated first using normalized conservative equation

$$\widetilde{S}(\widetilde{x},\widetilde{t}) = \widetilde{\Gamma}(\widetilde{x},\widetilde{t}) - \widetilde{q}(\widetilde{x},\widetilde{t}) \tag{35}$$

ACPD
15, 30321–30381, 2015

where $\widetilde{\Gamma}(\widetilde{x},\widetilde{t})$ is calculated using Eq. (28). Then, this term was represented using Eq. (9) as

$$\frac{2}{3}\widetilde{S}(\widetilde{x},\widetilde{t})\frac{\partial\widetilde{f}(\widetilde{x},\widetilde{t},\widetilde{\sigma}_j)}{\partial\widetilde{\sigma}_j}\approx\frac{\widetilde{f}\left(\widetilde{x},\widetilde{t},\widetilde{\sigma}_j+\frac{2}{3}\widetilde{S}\Delta\widetilde{t}\right)-\widetilde{f}\left(\widetilde{x},\widetilde{t},\widetilde{\sigma}_j\right)}{\Delta\widetilde{t}} \tag{36}$$

Therefore, at each time step the DSD $\widetilde{f}$ first was shifted left to the value $\frac{2}{3}\widetilde{S}\Delta\widetilde{t}$, where $\Delta\widetilde{t}$ is a small time increment chosen such that $\left|\frac{2}{3}\widetilde{S}_{\max}\Delta\widetilde{t}\right|\le\frac{\Delta\widetilde{\sigma}}{2}$. Then, the shifted DSD was remapped onto the fixed square radius grid $\widetilde{\sigma}_j$. We used Kovetz and Olund's (1969) remapping method, which conserves droplet concentration and LWC. After remapping, the differences between the new and old DSDs were recalculated. The new values of LWC within the DSD were determined using Eq. (26). MATLAB utility PDEPE automatically chooses the time step needed to provide stability of calculations.

5 Results of simulations

5.1 Full evaporation case

First, we consider the case $R = -1.5$, when all cloud water should evaporate. This process corresponds to the cloud dissipation caused by mixing with the entrained dry air. At the final stage, RH is expected to be uniform and negative in the entire volume.

Figure 3 shows spatial and time changes of $\widetilde{S}$ for $Da = 1$, 50 and 500. As seen from Fig. 3 at the final stage for all three cases $\widetilde{S} = -0.25$, which is in agreement with the analytical solution of Eq. (30). The final negative value indicates that all droplets were completely evaporated during mixing. In the case $Da = 1$ (Fig. 3a and b), two stages of supersaturation evolution can be identified. The first short stage, $t < 0.4\tau_{pr}$, is the period of inhomogeneous mixing during, when the gradients of RH persist. By end of the second stage of about $14\tau_{pr}$ the equilibrium state is reached. Thus, at small Da

ACPD
15, 30321–30381, 2015

both types of mixing take place during mixing between two volumes till the reaching the final equilibrium stage. Delimitation between mixing types in this case is somehow arbitrary and will be discussed in Sect. 5.3. In the cases of $Da = 50$ and $Da = 500$, spatial gradients exit during the entire period until reaching the equilibrium stage (approximately $50\tau_{pr}$ and $300\tau_{pr}$, respectively) (Fig. 3c–f). Therefore during these periods inhomogeneous mixing takes place.

Figure 4 shows spatial (upper row) and $\widetilde{x} - \widetilde{t}$ (lower row) changes of LWC for the same case as in Fig. 3. These diagrams demonstrate significant difference in the rates of evaporation at different Da numbers. Complete evaporation (LWC $= 0$) is reached at $Da = 1$, 50 and 500 at about 12, 22 and 120 relaxation times, respectively.

Analysis of Figs. 3 and 4 allows segregation of two characteristic times periods: (1) T_{mix} during this period spatial gradients of microphysical parameters persist and mixing is inhomogeneous, and (2) T_{ev}, during which droplet evaporation takes place. Both times are dimensionless and normalized using τ_0. Time T_{ev} is equal either to the time of total droplet evaporation (in the case of $R < -1.0$) or the time when the saturation deficit in the mixing volume becomes equal to zero (or close to zero if $R > -1.0$). Quantitative evaluations of T_{mix} and T_{ev} will be given in Sect. 5.3. At $\widetilde{t} < T_{mix}$, droplets in the mixing volume experience different saturation deficit. Toward the end of this stage, the saturation deficit becomes uniform over the entire mixing volume. At $Da = 1$, the homogenization of the saturation deficit and all microphysical variables takes place during a very short time of about $0.5\tau_{pr}$, and then the evaporation of droplets is assumed to take place under the same supersaturation conditions, so $T_{mix} \ll T_{ev}$.

Figure 4a and b shows that at $\widetilde{t} \approx 0.35$, normalized LWC drops down from 1 to 0.4. Since the average value of LWC in the initial volume is equal to 0.5 (see initial condition Eq. 27), 20 % of droplet mass evaporates during this short inhomogeneous period. Thus, despite a very short inhomogeneous mixing stage, evaporation plays an important role even at $Da = 1$.

Since the initial states are not homogeneous, there is always some period during which spatial inhomogeneities are present. With an increase in Da, the duration of

ACPD
15, 30321–30381, 2015

the inhomogeneous stage increases and the duration of the homogeneous stage decreases. In the case of $Da = 500$, homogenization of the saturation deficit requires $250\tau_{pr}$, which is twice as long as the total droplet evaporation time, i.e. $T_{mix} \approx 2T_{ev}$. This means that at $Da = 500$, the entire process of droplet evaporation takes place in the presence of spatial gradients of supersaturation. After full evaporation, spatial gradients of the water vapour mixing ratios remain. Such mixing can be regarded as inhomogeneous.

At $Da = 50$, the time of complete evaporation is approximately equal to the time of supersaturation homogenization, i.e. $T_{mix} \approx T_{ev}$. In this case, as in the case of $Da = 500$, the process of droplet evaporation occurs in an environment of a non-uniformly distributed saturation deficit and also can be regarded as inhomogeneous.

The differences in the process of droplet evaporation at different Da can be seen in Fig. 5. Figure 5 shows the relationships between $\widetilde{N}$ and $\widetilde{q}$ plotted with a certain time increment, so that each symbol on the diagrams corresponds to a particular moment of time. The set of these symbols forms curves. Each panel of Fig. 5 shows three such curves corresponding to different $\widetilde{x}$: the centre of an initially cloud volume ($\widetilde{x} = 1/4$); the centre of the mixing volume ($\widetilde{x} = 1/2$); and the centre of an initially droplet-free volume ($\widetilde{x} = 3/4$). The directions of time increase are shown by arrows along the corresponding curves in the Fig. 5. The initial points of the curves corresponding to $\widetilde{t} = 0$ are characterized by values $\widetilde{q} = 1$ and $\widetilde{N} = 1$ at $\widetilde{x} = 1/4$, and by values $\widetilde{q} = 0$ and $\widetilde{N} = 0$ at $\widetilde{x} = 3/4$.

The behaviour of the $\widetilde{N}$–$\widetilde{q}$ relationships provides important information about the mixing process. At $\widetilde{t} < T_{mix}$, there are spatial gradients of $\widetilde{N}$ and $\widetilde{q}$, i.e. $\widetilde{N}$ and $\widetilde{q}$ are different at different $\widetilde{x}$. This means that the three curves at $\widetilde{t} < T_{mix}$ are different and do not coincide. At $\widetilde{t} > T_{mix}$, the spatial gradients of $\widetilde{N}$ and $\widetilde{q}$ disappear and the three curves coincide. So, when the curves do not coincide, mixing is inhomogeneous, and the coincidence of the curves indicates that mixing becomes homogeneous. In Fig. 5a and b ($Da = 1$ and 5 respectively), the curves coincide at point A, corresponding to time $\widetilde{t} = T_{mix}$.

ACPD
15, 30321–30381, 2015

Figure 5a and b shows that at $Da = 1$ and $Da = 5$ the process of mixing consists of two stages: inhomogeneous and homogeneous. The time instance $\widetilde{t} = T_{\mathrm{mix}}$ separates these two stages. In turn, the period of homogeneous evaporation can be separated into two parts. In the first part, droplets evaporate only partially and $\widetilde{q}$ decreases under the same droplet concentration. This stage is very pronounced at $Da = 1$, when $\widetilde{q}$ decreases from about 0.4 to 0.1 at the unchanged droplet concentration. At the later stage, when $\widetilde{q} < 0.1$, droplets evaporate totally, beginning with smaller ones, so both droplet concentration and $\widetilde{q}$ rapidly decrease to zero. At $Da = 5$ (Fig. 5b), at the stage of homogeneous evaporation (that begins at point "A") a decrease in $\widetilde{q}$ is accompanied by a decrease in $\widetilde{N}$.

At $Da = 50$ (Fig. 5c), curves corresponding to different values of $\widetilde{x}$ do not coincide, except at the final point "F", where $\widetilde{N} = 0$ and $\widetilde{q} = 0$. This means that horizontal gradients exist and mixing is inhomogeneous till the final equilibrium state is reached. Droplets penetrating into the dry volume begin evaporating, so only a small fraction of droplets reaches the centre of the dry volume, as seen in Fig. 5c, $\widetilde{x} = 3/4$ (black curve). Accordingly, at $\widetilde{x} = 3/4$ droplet concentrations and $\widetilde{q}$ reach their maxima (of 0.1 and 0.05, respectively) and then decrease to zero. In the case of $Da = 500$ (Fig. 5d), all droplets evaporate before reaching the centre of the dry volume, indicating an extreme spatial inhomogeneity of droplet evaporation. Hence, only two curves for $\widetilde{x} = 1/4$ and $\widetilde{x} = 1/2$ are seen in Fig. 5d.

Figure 5 also shows that the slopes of the curves describing the $\widetilde{N}$–$\widetilde{q}$ relationships are different at different values of $\widetilde{x}$, and that they change over time. At large Da, the slopes of the curves describing the dependencies $\widetilde{N}$–$\widetilde{q}$ in the initially cloud volume are close to linear. However, the slope at a high value of $\widetilde{q}$ is still lower than that at a low value of $\widetilde{q}$. This can be attributed to the fact that when $\widetilde{q}$ is large, it decreases faster than concentration $\widetilde{N}$ because of the presence of partial droplet evaporation. At the end of the process, when $\widetilde{q}$ is small, $\widetilde{N}$ decreases faster than $\widetilde{q}$, because concentration is determined by the smallest droplets, while $\widetilde{q}$ is determined by larger droplets.

ACPD
15, 30321–30381, 2015

It was discussed in Pt1 that according to the classical concept, for extremely inhomogeneous mixing the ratio of different DSD moments (e.g. N/q) remains constant. For the dimensionless $\widetilde{N}$ and $\widetilde{q}$ the scattering points should be aligned along the 1 : 1 line. Therefore, the closeness of particular cases to the classical inhomogeneous mixing can be determined from deviation of $\widetilde{N}$–$\widetilde{q}$ curve from 1 : 1 line. One can see that in case $Da = 500$ the $\widetilde{N}$–$\widetilde{q}$ relationship is closer to linear.

Despite the fact that at $R < -1$ all droplets within the mixing volume evaporate, it is interesting to follow the DSD evolution during this process. Figure 6 shows the time evolution of a normalized DSD at $Da = 1$ and $Da = 50$. One can see a substantial difference in DSD evolutions at different Da. In the case of $Da = 1$, different DSDs very rapidly form at different values of $\widetilde{x}$ (panel a). The widest DSD occurs at $\widetilde{x} = 1$, i.e. at the outer boundary of the initially non-cloud volume. This is natural, because the supersaturation deficit is greatest at $\widetilde{x} = 1$. At $\widetilde{t} > T_{\text{mix}} \approx 0.4$ DSDs become similar at all values of $\widetilde{x}$ (Fig. 6b). The DSD width continues to increase due to partial droplet evaporation. This time corresponds to the horizontal segment of the $\widetilde{N}$–$\widetilde{q}$ relationship in Fig. 5a. Figure 6c shows the DSD at the stage when a decrease in LWC is accompanied by a decrease in number concentration. The corresponding point at the $\widetilde{N}$–$\widetilde{q}$ diagram at this time instance is quite close to the point "F" at which $\widetilde{N} = 0$ and $\widetilde{q} = 0$.

In the case of $Da = 50$, DSDs are different at different $\widetilde{x}$ during the entire period of mixing. One can see that while DSDs at $\widetilde{x} > 0.5$ are wide and droplet evaporation is accompanied by a shift of DSD maximum to smaller droplet radii (a feature typically attributed to homogeneous mixing), the DSD maximum at $\widetilde{x} < 0.5$ (originally cloud volume) shifts toward smaller radii only slightly until $\widetilde{t} = 3.17$ (Fig. 6e). Further droplet evaporation leads either to total droplet evaporation (at $\widetilde{x} \geq 0.5$) or to a shift of DSDs to small droplet sizes (panel f). The maximum droplet concentration remains at $\widetilde{x} = 0$. The difference in DSDs at different $\widetilde{x}$ occurs because of a lack of correspondence between curves representing different $\widetilde{N}$–$\widetilde{q}$ relationships, as shown in Fig. 5c. Figure 6 shows that DSD shapes evolve substantially over time, although the final state is characterized by total cloud droplet evaporation.

ACPD
15, 30321–30381, 2015

5.2 Partial evaporation case

5.2.1 Evolution of microphysical parameters at different *Da* and *R*

Now we shall consider the process of mixing when $R > -1$, i.e. in cases when not all the droplets evaporate. Figure 7 shows horizontal profiles of a normalized supersaturation at different *Da* and *R*. One can see that in all cases, the final state occurs when the equilibrium supersaturation $\widetilde{S} = 0$ (RH = 100 %). However, this final value is reached quite differently, depending on *Da*. At $Da = 1$, rapid mixing leads to the formation of spatially homogeneous humidity and supersaturation during a time period of less than a fraction of τ_{pr}. Then, supersaturation within the entire volume grows by the evaporation of droplets, which are uniformly distributed within the total volume. This process (homogeneous mixing) was considered in detail in Pt2.

At $Da = 500$, changes in supersaturation take place largely within an initially dry volume. RH in an initially cloud volume undergoes only small changes. This process agrees well with the classical concept of extreme inhomogeneous mixing. Note, however, that a strong gradient of supersaturation remains for a long time (tens of τ_{pr}) within an initially drop-free volume. At $Da = 50$, the situation is intermediate. Mixing is strong enough to decrease RH in an initially cloud volume, but spatially uniform RH is established in about $5–10\tau_{pr}$, increasing with an increase in $|R|$. After this time instance, mixing takes place according to the homogeneous scenario.

Figure 8 shows horizontal profiles of normalized LWC at different *Da* and *R*. At the same *R*, the final equilibrium values of LWC are the same, as follows from Eq. (30); LWC decreases with an increase in $|R|$. A decrease in the LWC in a cloud volume is caused largely by the process of the diffusion of droplets from a cloud volume to an initially dry volume for any *Da*.

Evaporation in a cloud volume at $Da = 500$ is small because $\widetilde{S}$ is high in cloud volumes during mixing (Fig. 7). At $Da = 1$, the process of spatial homogenization takes place for fractions of τ_{pr}, i.e. $T_{mix} < 1$. Then, during the relatively lengthy period of $10\tau_{pr}$, evaporation decreases LWC over the entire mixing volume, as occurs in homogeneous

ACPD
15, 30321–30381, 2015

mixing. At $Da = 50$, spatial homogenization takes place during about $T_{mix} \approx 15$. This is slightly shorter time than it takes to establish the final equilibrium stage T_{tot}. Different Da's reach equilibrium at different times. The process of reaching a final uniform LWC lasts $100\tau_{pr}$ in the case of $Da = 500$ and about τ_{pr} in the case of $Da = 1$.

Figure 9 shows profiles of normalized droplet concentrations at different Da and R. In contrast to LWC, the final concentration depends jointly on Da and R. Hence, profiles at different Da can have different shapes at the same value of R. At $R = -0.1$ (which corresponds to high RH in an initially dry volume) there is no total droplet evaporation, so the final normalized droplet concentration is equal to $\widetilde{N} = 1/2$. This means that all droplets in the initially cloud volume are now uniformly distributed between cloud and dry volumes. At larger $|R|$ (lower RH in an initially dry volume), some droplets totally evaporate. The final concentration decreases with an increase in the Da.

The physical implication of such dependence is clear. At low Da, fast mixing leads to the formation of a uniform RH throughout the entire volume, and this affects all droplets. At high Da, RH in an initially dry volume remains low for a long time, and droplets that penetrate can evaporate. Therefore, the fraction of fully evaporated droplets increases with Da. In the example presented in Fig. 9, at $R = -0.1$ there is no Da at which a full evaporation of individual droplets takes place. At $R = -0.3$ a decrease in droplet concentration takes place only at $Da = 500$. At $R = -0.5$ a decrease in droplet concentration takes place already at $Da \geq 50$.

The comparative contributions of different factors in establishing the final states of mixing is well seen in Fig. 10, which shows the relationships between normalized concentration and normalized LWC at three values of $\widetilde{x}$: 1/4 (centre of cloudy volume), 1/2, and 3/4 (centre of initially dry volume) at $R = -0.5$ and different values of Da. Figure 10 is analogous to Fig. 5, but plotted for $R > -1$.

In case of $Da = 1$ the mixing is very fast, which leads to a rapid decrease in LWC and concentration in the initially cloud volume and an increase of these quantities in the initially dry volume. As a result of the rapid mixing and homogenization, all curves coincide at point "A" (left panel). After this time instance, spatial homogeneous evaporation

ACPD
15, 30321–30381, 2015

takes place. Since at $Da = 1$ only partial, but not total, evaporation takes place, droplet concentration remains unchanged even while LWC decreases. In cases $Da = 50$ and 500, three curves coincide in one final point "F" only. In cases of $Da = 500$ the relationship between droplet concentration and mass becomes more linear (blue curve). Recall that linear dependence is associated with concept of extreme inhomogeneous mixing (see Pt1). Comments made about closeness of the $\widetilde{N}$–$\widetilde{q}$ relationship to the line 1 : 1 as a measure of the inhomogeneity of mixing made for the case $R < -1$ are valid also in the case $R > -1$.

5.2.2 Evolution of DSDs and their parameters

Figure 11 presents examples of DSD evolution in the centers of the initially cloud volume ($\widetilde{x} = 1/4$) (upper row) and in an initially dry volume ($\widetilde{x} = 3/4$) at $R = -0.5$ and different values of Da. We note several typical properties of the DSDs. Rapid mixing at $Da = 1$ (left column) leads to the fact that DSDs become similar in both volumes already at $t = 0.317\tau_{pr}$ (black lines). Further evolution is similar in both volumes and is characterized by a shifting and broadening of the DSD toward small droplet size. Such a shift means that a decrease in mass under constant droplet concentration, which is typical of homogeneous mixing.

Note that initially monodisperse DSDs become polydisperse. The mechanism of the DSD broadening at $Da = 1$ is illustrated in Fig. 12, where the DSD at the earlier, inhomogeneous stage at different $\widetilde{x}$ is shown. One can see in Fig. 12 that in the very short periods when the spatial gradient of saturation deficit exists, droplets moving by diffusion to initially dry volume partially evaporate, becoming smallest at $\widetilde{x} = 1$. So, a polydisperse DSD forms. The mixing leads then to a spatial homogenization of DSDs, as seen in the right panel of Fig. 12.

In the cases $Da = 50$ and 500, the shapes of DSD substantially differ from those at $Da = 1$. There are two main differences: the peak of the distribution shifts only slightly ($Da = 50$) or does not shift at all ($Da = 500$). At the same time, the DSD develops a long tail of small droplets. Since the rate of mixing at these values of Da is slow, droplets

ACPD
15, 30321–30381, 2015

penetrating to a greater distance into the initially dry volume remain there for long time and decrease to smaller sizes. As a result, at moderate and large *Da*, polydisperse DSDs form with droplet sizes ranging from zero to 1. The formation of a long tail of small droplets in the case of inhomogeneous mixing was simulated in direct numerical simulation (DNS) by Kumar et al. (2012), as well as by using the "explicit-mixing parcel model" (EMPM) (Krueger et al., 1997; Su et al., 1998; Schlüter, 2006).

Figure 13 shows the spatial dependencies of the DSD dispersion (ratio of DSD r.m.s. width and mean radius) at different time instances, and the values of *Da* and *R*. One can see that the dispersion increases with an increase in *Da* and $|R|$. The reason for such behavior is related to that the DSD broadening toward small size end increases with an increase in *Da* and $|R|$. The DSD dispersion increases with time and with an increase in $\widetilde{x}$ (i.e. further into the dry volume). At the same time, spatial homogenization takes place, so at the final state at $R = -0.5$ the DSD dispersion reaches 0.11 at $Da = 1$ and about 0.2 at $Da = 50$ and $Da = 500$.

Observed DSD dispersion in different clouds typically range from 0.1 to 0.4 (Khain et al., 2000; Martin et al., 2004; Prabha et al., 2012). Such DSD dispersion may be explained by in-cloud nucleation (e.g. Khain et al., 2000; Pinsky and Khain, 2002), spatial averaging along aircraft traverses (Korolev, 1995) and non-symmetry in droplet nucleation/denucleation (Korolev, 1995). As seen from Fig. 13, such dispersion may be caused by mixing at cloud edges at moderate and large *Da*. So, inhomogeneous mixing leads to DSD broadening.

The effective radius is an important DSD characteristic. According to the classical concept, the effective radius is expected to remain unchanged during extreme inhomogeneous mixing, whereas during homogeneous mixing the effective radius is anticipated decreasing. Figure 14 shows the spatial dependencies of the effective radius at different time instances and values of *Da* and *R*. At $R = -0.1$ (high RH in the environmental volume) the effective radius is similar for all values of *Da*. So, at high *R*, the behaviour of the effective radius does not allow us to distinguish the mixing type.

ACPD
15, 30321–30381, 2015

At a given R, the final effective radii increases with increasing Da. For instance if $R = -0.5$, the effective radius in the final state differs from the initial one by less than 6 % at $Da = 500$, while at $Da = 1$ it decreases by 20 %. Note that in cases of moderate and high Da, large gradients of the effective radius exist during the mixing process. Note, however, that the gradient is high only in an initially droplet-free volume, where the effective radius decreases significantly due to the evaporation of droplets. Besides, effective droplet radius in the initially dry volume growth very rapidly, so at high Da during most of the mixing time effective radius within mixing volume is close to the initial value in the cloudy volume. This result agrees in general with the classical concept of extreme inhomogeneous mixing.

5.3 Delimiting between mixing types

Typically, the value of the Da number is used as a criterion to distinguish between types of mixing. $Da = 1$ is usually used as a boundary value separating homogeneous and inhomogeneous types of mixing. As shown in the previous section, the process of mixing may consist of two stages. Mixing always begins at an inhomogeneous stage. In the course of mixing, the initial spatial gradients decrease and the air volumes either become identical or remain different. In the case of the former, the inhomogeneous stage is replaced by a homogeneous one. In cases in which inhomogeneity exists until the equilibrium state is established, the entire period of mixing is inhomogeneous. Both mixing stages can be characterized by duration, change in droplet concentrations or LWCs, or other quantitative characteristics. These characteristics are some function of two non-dimensional parameters R and Da, which can be calculated and used for distinguishing between mixing types. Since mixing between volumes may change from inhomogeneous to homogeneous before reaching the equilibrium state, there is a necessity to use some quantitative criteria to delimit mixing types. Below, we carry out such a delimitation for the important case when $R > -1$, which correspond to partial evaporation of droplets by the end of mixing.

ACPD
15, 30321–30381, 2015

5.3.1 Characteristic time periods of the mixing process

One can define three characteristic periods: (a) mixing period T_{mix}, during which spatial gradients are smoothened. This period also can be referred to as the period of homogenization, (b) evaporation period T_{ev}, during which $S < 0$ and droplets evaporate. As soon as the saturation is reached, the evaporation is terminated, (c) total mixing period T_{tot}, which is the period till the final equilibrium stage is reached. All three times are dimensionless quantities in the study.

We use solution Eq. (28) for conservative function $\widetilde{\Gamma}(\widetilde{x},\widetilde{t})$ to define quantitatively the mixing duration time T_{mix}. The deviation of solution from its final value $\Delta\widetilde{\Gamma} = \widetilde{\Gamma}(\widetilde{x},\widetilde{t}) - \widetilde{\Gamma}(\widetilde{x},\infty)$ when $\widetilde{t} \to \infty$ can be approximately estimated using the first term of the series expansion as

$$\left|\Delta\widetilde{\Gamma}\right|_{max} \approx \left|(1-R)\frac{\sin(\pi/2)}{\pi/2}\exp\left(-\frac{\pi^2\widetilde{t}}{Da}\right)\cos\left(\pi\widetilde{x}\right)\right|_{max} = (1-R)\frac{2}{\pi}\exp\left(-\frac{\pi^2\widetilde{t}}{Da}\right) \tag{37}$$

From Eq. (37) the estimation of T_{mix} can be written as

$$T_{mix} = -\frac{Da}{\pi^2}\ln\left[\frac{\pi}{2(1-R)}\left|\Delta\widetilde{\Gamma}\right|_{max}\right] \tag{38a}$$

Let us set the value of maximal deviation $\left|\Delta\widetilde{\Gamma}\right|_{max} = 0.02$. This is a small value as compared to the initial jump of function $\widetilde{\Gamma}$, which is equal to $1-R$. In this case, the duration of the non-homogeneous stage is evaluated as

$$T_{mix} = -\frac{Da}{\pi^2}\ln\left[\frac{0.01\pi}{1-R}\right] \tag{38b}$$

ACPD
15, 30321–30381, 2015

Several studies evaluate evaporation time for droplets of a particular size using the equation for diffusion growth (e.g. Lehmann et al., 2009). In our study, the evaporation time duration T_{ev} is defined as the period during which maximal supersaturation deviation from zero exceeds some small value $\left|\Delta\widetilde{S}\right|_{max} = 0.02$

$$\left|\widetilde{S}(\widetilde{x}, T_{ev})\right| \le \left|\Delta\widetilde{S}\right|_{max} = 0.02 \quad (39)$$

Criterion Eq. (39) is somehow subjective. An advantage of this criterion as compared to that used by Lehmann et al. (2009) is that it characterizes evaporation of the droplets population taking into account simultaneous increase in supersaturation, but not of individual droplets of particular size under constant S.

At the end of the mixing process both thermodynamic and diffusion equilibriums are reached. Accordingly, the total time of mixing T_{tot} is evaluated as the maximum of the two times needed to achieve equilibrium $T_{tot} = \max\{T_{mix}, T_{ev}\}$. Note that all three characteristic time periods are normalized on the phase relaxation time, and therefore depend on two non-dimensional parameters R and Da. The contours of the characteristic time durations T_{mix}, T_{ev} and T_{tot}, on Da–R diagrams are shown in Fig. 15.

As follows from Eq. (38b), T_{mix} is proportional to Da. The dependence of T_{mix} on R is not very strong, so T_{mix} slightly decreases with an increase in R. This can be attributed to the fact that the lower R, the smaller the initial inhomogeneity of function Γ and the smaller the time to align this inhomogeneity. At small Da (high rate of homogenization of the volume), T_{ev} depends largely on R. At large Da, T_{ev} depends substantially on Da, since the rate of evaporation depends on the number of droplets that diffuse to the drier parts of the mixing volume. A comparison of Fig. 15c with Fig. 15a and b shows that at small Da, time T_{tot} is determined by T_{ev}, while at large Da, T_{tot} is determined by T_{mix}.

ACPD
15, 30321–30381, 2015

5.3.2 Delimitation between the types of mixing

One can propose several criteria of delimitation between the types of mixing. We consider these criteria for the case $R > -1$. As discussed above, mixing always starts as inhomogeneous. Then it can convert to homogeneous or remain inhomogeneous till the establishing the final state equilibrium state. It is reasonable to refer the latter case as inhomogeneous mixing. At small Da, the process of homogenization takes place during $T_{mix} < T_{tot}$. The time fraction λ_1 of the inhomogeneous stage can serve as a criterion of the definition of homogeneous mixing. This fraction can be defined as

$$\lambda_1 = \frac{T_{mix}}{T_{tot}} \tag{40}$$

The case $\lambda_1 \le 0.5$, i.e. when most time the mixing takes place according the homogeneous scenario is reasonable to regard as homogeneous. In case $\lambda_1 = 1$, the mixing is inhomogeneous, as mentioned above. If $\lambda_1(R, Da)$ changes within the range $0.5 < \lambda_1 \le 1$, the mixing is reasonably be refer to as intermediate. The criteria Eq. (40) depends on the non-dimensional parameters R and Da. Figure 16a shows these three zones on the Da–R plane. Note that at very small R, the duration time of phase transition is negligibly small. According to criteria Eq. (40), the mixing in this case should be considered as inhomogeneous, irrespective of the value of Da.

Another criterion of delimitation between mixing types can be determined from a comparison of the rates of LWC change during different mechanisms. Let us define the mean normalized LWC as integral $\left\langle \widetilde{q}(\widetilde{t}) \right\rangle = \int_0^1 \widetilde{q}(\widetilde{x}, \widetilde{t}) D\widetilde{x}$. The initial mean LWC is equal to $\langle \widetilde{q}(t=0) \rangle = \frac{1}{2}$. The final equilibrium LWC is equal to $\langle \widetilde{q}(t=\infty) \rangle = \frac{1}{2}(1+R)$ (see Eq. 30). The total amount of liquid water that evaporates in the course of mixing can be quantified by the difference between these two values $\langle \widetilde{q}(t=0) \rangle - \langle \widetilde{q}(t=\infty) \rangle = -\frac{1}{2}R$. The amount of liquid water evaporated in the course of the first, inhomogeneous stage of mixing is calculated from the equation $\langle \widetilde{q}(t=0) \rangle - \langle \widetilde{q}(T_{mix}) \rangle = \frac{1}{2} - \langle \widetilde{q}(T_{mix}) \rangle$. Now, one

ACPD
15, 30321–30381, 2015

can define another possible criterion of the delimitation between the types of mixing, the parameter λ_2 which is a ratio of

$$\lambda_2 = \frac{\langle\widetilde{q}(t=0)\rangle - \langle\widetilde{q}(T_{\mathrm{mix}})\rangle}{\langle\widetilde{q}(t=0)\rangle - \langle\widetilde{q}(t=\infty)\rangle} = \frac{2\langle\widetilde{q}(T_{\mathrm{mix}})\rangle - 1}{R} \tag{41}$$

This ratio characterizes the fraction of liquid water that evaporates at the initial inhomogeneous stage. Condition $\lambda_2 < 0.5$ in this case can be associated to homogeneous mixing, while condition $0.5 \le \lambda_2 < 1$ corresponds to intermediate mixing. We regard the case $\lambda_2 = 1$ as inhomogeneous mixing. Of course, criterion λ_2 depends on both non-dimensional parameters R and Da. Figure 16b illustrates the delimitation between the types of mixing on the Da–R plane according to the criterion λ_2.

A comparison of Fig. 16a and b shows a similar separation of the Da–R plane into three zones corresponding to homogeneous, intermediate and inhomogeneous mixing. At the same time, the boundaries separating these three zones are different for different criteria. However, one can conclude that at Da smaller than 4–10 and $R < -0.1$, mixing can be considered as homogeneous, and at Da larger than several tens mixing can be considered inhomogeneous.

In literature terms "inhomogeneous mixing" (Burner and Brenguier, 2007) and "extremely inhomogeneous mixing" (Lehmann et al., 2009; Gerber et al., 2008; Pt1) are used to denote the mixing regime when the relationship between normalized values N and q is represented by a straight 1 : 1 line, which is equivalent to the constant mean volume radius (in some studies effective radius is used instead of mean volume one). According to the definition in the present study, extremely inhomogeneous mixing is the limiting case of inhomogeneous mixing when $Da \to \infty$. Despite the fact that the extremely inhomogeneous mixing is only some idealization, which is never can realize in reality, our approach allows to evaluate to what extent the mixing can be regarded to as extremely inhomogeneous. The measure of inhomogenity of mixing is the closeness of the $\widetilde{N}$–$\widetilde{q}$ relationship to the 1 : 1 straight line (see discussion related to Figs. 5 and 10).

ACPD
15, 30321–30381, 2015

Figure. 17a shows r.m.s. distance between the $\widetilde{N}$–$\widetilde{q}$ relationship and the 1 : 1 straight line depending on Da and R. These dependences were calculated from set of points $\widetilde{N}_i, \widetilde{q}_i$ uniformly distributed in spatial interval $0/1$ and time interval $0/T_{\text{tot}}$. The equation for estimation is $\delta = \sqrt{\frac{1}{2M}\sum_{i=1}^{M}\left(\widetilde{N}_i - \widetilde{q}_i\right)^2}$, where M is the total number of points. This distance corresponds to r.m.s. deviation of normalized mean volume radius from 1. The dependences of last deviation on Da and R, which were estimated as $\delta/3$ are shown in the Fig. 17b. This estimation is based on the fact that mass of drops is proportional to the cube of the mean volume radius. As expected, the distance decreases with an increase in Da. At large R all curves coincide indicating degenerative case when type of mixing becomes indistinguishable.

We conventionally assume that the value of the r.m.s deviation of normalized mean volume radius from the initial radius equal to 0.02 is reasonably small to determine the boundary of the extremely inhomogeneous mixing zone. The value 0.02 corresponds to droplet radii deviation of a few tenths of a micron, which is very small, and in in-situ measurements this case would always be attributed to extremely inhomogeneous mixing. This boundary is plotted in the Fig. 16 by broken line. The line shows that the mixing characterized by Da exceeding several hundred can be attributed to extreme inhomogeneous mixing. Note that between the boundary separating inhomogeneous mixing from the intermediate one and the zone of extremely inhomogeneous mixing there exists a wide zone of inhomogeneous mixing where the mean volume (or effective) radius may drop by 10 % and more (Fig. 14), dispersion of DSD is substantial and the tail of small droplets is significant (Fig. 11). Mixing diagrams widely used for analysis of observed data ($N - q$ dependences in final equilibrium state of mixing) do not contain this zone, so this zone have not been designed and studied yet.

ACPD
15, 30321–30381, 2015

6 Summary and conclusions

In this study, the process of inhomogeneous turbulent mixing is investigated using a simple a 1-D model of mixing between saturated cloud volume and undersaturated droplet-free volume. The process of mixing is simulated by solving a diffusion-evaporation equation written in non-dimensional form. For simplicity, the initial volumes of cloudy and environmental air were assumed to be equal, and the initial DSD in the cloudy volume was assumed to be monodisperse.

The analysis of the diffusion-evaporation equation shows that the process of mixing and the final equilibrium state depend on two non-dimensional parameters. The first parameter R is proportional to the ratio between the saturation deficit in an initially dry volume and the initial liquid water content in a cloudy volume. At $R < -1$, the final state is characterized by total droplet evaporation and a spatially homogeneous saturation deficit. Such a case corresponds to the dissipation of cloudy volume that mixed with dry out-of-cloud air. In the case of $R > -1$, the final state is characterized by the existence of droplets and a zero saturation deficit (RH = 100 %). In this case the cloud volume is increased after mixing with the entrained air. At small values of parameter $|R|$ (e.g., when RH in the entrained volume is close to 100 %), the effect of droplet evaporation on microphysics is small, and, formally, the mixing should be regarded as extremely inhomogeneous. Strictly speaking this is a degenerate case, when there is no difference between homogeneous and inhomogeneous mixing. At $R = 0$, droplets turn into a passive admixture and their turbulent diffusion will be the same as other thermodynamic parameters.

The second parameter is the Damkölher number, Da, which is the ratio between characteristic times of mixing and phase relaxation. This parameter compares the rates of spatial diffusion and evaporation processes. The analysis was performed within a wide range of Da (from 1 to 500) and R (from −1.5 to −0.1). The final LWC and humidity in the volume are determined by the mass conservation and they do not depend

ACPD
15, 30321–30381, 2015

on *Da* (see also Pt1). At the same time, the droplet concentration, as well as the shape and parameter of DSDs, strongly depend on *Da*.

It is shown that the process of mixing of initially different volumes consists of two stages and can be characterized by two times: the time during which microphysical characteristics become uniform over the total mixing volume T_{mix}, and the time during which a zero saturation deficit is reached (in cases of $R > -1$), T_{ev}. At times $\widetilde{t} < T_{mix}$, the spatial gradients of microphysical values remain and the mixing regime can be regarded as inhomogeneous. At times $\widetilde{t} > T_{mix}$, evaporation takes place (if it does at all) within a spatially homogeneous medium, so all droplets experience the same saturation deficit. Such a regime can be regarded as homogeneous. It is shown, therefore, that at small *Da* mixing between two volumes that starts as inhomogeneous can turn out to be homogeneous to the end of mixing process.

This finding made desirable (and possible quantitatively) to perform delimiting between mixing types. We presented two quantitative criteria on the *Da*–*R* plane that allow us to delimit three mixing regimes: homogeneous, intermediate and inhomogeneous. These criteria are based on comparison of characteristic duration times of mixing and the evaporation rates. These criteria showed that at *Da* less than about 5, mixing can be regarded as homogeneous, i.e. the main microphysical changes take place during the homogeneous stage. At $5 < Da < 30/50$ the changes in microphysical parameters are larger at the inhomogeneous stage than that at the homogeneous stage. In this case, the mixing can be regarded as intermediate. Last, at *Da* larger than several tens, the spatial microphysical gradients remain till the reaching of the final equilibrium stage. In this case, the mixing can be regarded as inhomogeneous. At *Da* larger than a few hundred the deviations from predictions of classical concept become relatively small. Mixing at such high *Da* can be attributed to extremely inhomogeneous.

Overall, the results of the present study are in line with the classical concepts regarding homogeneous and inhomogeneous mixing types. However, several important points emerge from our work that complement and clarify these assumptions. A com-

ACPD
15, 30321–30381, 2015

parison of the classical concepts (see Pt1) and the present study is presented in Table 2.

We comment on Table 2 as follows.

a. In contrast to many studies that analyze or assume the final, equilibrium state of mixing (Barnet and Brenguier, 2007; Gerber et al., 2008; Morrison and Grabowski, 2008; Hill et al., 2009) we consider the time-dependent processes of mixing and evaporation. The duration of the mixing process can last several minutes at moderate and high *Da*. In observations, we see mostly non-equilibrium stages, which may help to account for a quite-wide scattering of mixing diagrams even under the same values of *Da* (e.g., Lehmann et al., 2009). Note that time dependent mixing was also considered in several studies (e.g. Baker et al., 1980; Baker and Latham, 1982; Jeffery and Reisner, 2006; Krueger et al., 1997; Kumar et al., 2012).

b. It is also shown that the slopes of the $\widetilde{N}$–$\widetilde{q}$ (droplet concentration-LWC) relationship tends to the 1 : 1 line with increase in *Da*. The closeness of the relationship to this straight line can be considered as closeness to the extreme inhomogeneous mixing in terms of classical concept (see Pt1). It is found that the slope of the $\widetilde{N}$–$\widetilde{q}$ relationship depends on the LWC and, accordingly, on time. At large LWC, $\widetilde{q}$ changes with time faster than $\widetilde{N}$, while at low LWC, the concentration changes faster. Such differences were found in a numerical simulation of stratiform clouds in the vicinity of a cloud top (Magaritz-Ronen et al., 2015). Types of mixing are typically separate into homogeneous and extremely inhomogeneous. In this study it is shown that there are the wide ranges of *Da* and *R*, when mixing can be attributed to the intermediate and to inhomogeneous (but not extremely inhomogeneous). Within this zone effective radius can change by more than by 10–15 %. Standard mixing diagrams do not include this zone. To our knowledge, this zone was never investigated despite the fact that many in-situ measurements seem to belong to this zone.

ACPD
15, 30321–30381, 2015

c. Many studies assume existence of pure homogeneous mixing, when an initially monodisperse DSD would remain monodisperse. Our study shows that at the very beginning mixing is always inhomogeneous. This inhomogeneous stage leads to the formation of a polydisperse DSD, the width of which increases in the course of droplet evaporation. So, even at $Da = 1$, a monodisperse spectrum becomes polydisperse.

d. It is shown that at small *Da*, process of mixing includes inhomogeneous and homogeneous stages. So, mixing changes its type during the mixing process.

e. The classical concept assumes that the effective radius always decreases during homogeneous mixing. In the present study, where we considered an initially monodisperse DSD, this conclusion proved largely valid, with the exception of the cases of small R. However, in Pt2, it was shown that depending of the shape of DSD, the effective radius can decrease, remain constant or increase during homogeneous mixing. Thus, a decrease in the effective radius during the mixing process cannot always be considered an indication of homogeneous mixing.

f. It is generally assumed that droplet concentration remains unchanged during homogeneous mixing. In the present study, as well as in Pt2, it is shown that since mixing leads to a polydisperse DSD, the smallest droplets may totally evaporate. In the case of $R < -1$, the DSD becomes very wide and all droplets, beginning with the smaller ones, evaporate.

g. It is widely assumed that inhomogeneous mixing does not alter DSD shape, but rather only decreases droplet concentration. The present study showed that inhomogeneous mixing may significantly change the DSD shape. DSDs turned out to be quite different in different regions of mixing volumes. The main feature is broadening of DSD toward small droplets with relative dispersion up to 0.2–0.3. These values are quite close to those observed in atmospheric clouds (Khain et al., 2000). Such elongated tails of small droplets have been simulated by Schlüter

ACPD
15, 30321–30381, 2015

(2006), who used the EMPM to describe turbulent diffusion (Kruger et al., 1997; Su et al., 1998) and by Kumar et al. (2012) using DNS. So, we see that the formation of a polydisperse DSD is a natural result of inhomogeneous mixing. Inhomogeneous mixing, then, is an important mechanism in the DSD broadening. The significant role of mixing on the DSD shape has been identified in many studies, beginning with Warner (1973).

h. It has been long thought that the effective radius remains constant in inhomogeneous mixing. Our results indicate that, indeed, in the final equilibrium stage at comparatively high RH in a non-cloudy air volume, the effective radius is close to that found in an initially cloudy volume (especially at high *Da*). At the same time, the results show that during mixing, the effective radius varies in size, and is smaller in initially non-cloudy volumes. The effective radius also changes substantially in cases of low RH in the entrained volume at which most (or all) droplets evaporate by mixing.

Acknowledgements. This research was supported by the Israel Science Foundation (grant 1393/14), the Office of Science (BER), US Department of Energy Award DE-SC0006788 and the Binational US-Israel Science Foundation (grant 2 010 446). Korolev's participation was supported by Environment Canada.

References

Baker, M. and Latham, J.: The evolution of droplet spectra and the rate of production of embryonic raindrops in small cumulus clouds, J. Atmos. Sci., 36, 1612–1615, 1979.

Baker, M. B. and Latham, J.: A diffusive model of the turbulent mixing of dry and cloudy air, Q. J. Roy. Meteor. Soc., 108, 871–898, 1982.

Baker, M., Corbin, R. G., and Latham, J.: The influence of entrainment on the evolution of cloud drop spectra: I. A model of inhomogeneous mixing, Q. J. Roy. Meteor. Soc., 106, 581–598, 1980.

Burnet, F. and Brenguier, J.-L.: Observational study of the entrainment-mixing process in warm convective cloud, J. Atmos. Sci., 64, 1995–2011, 2007.

ACPD
15, 30321–30381, 2015

Blyth, A. M., Choularton, T. W., Fullarton, G., Latham, J., Mill, C. S., Smith, M. H., and Stromberg, I. M.: The Influence of entrainment on the evolution of cloud droplet spectra, 2. Field experiments 5 at Great Dun Fell, Q. J. Roy. Meteor. Soc., 106, 821–840, 1980.
Boffetta, G. and Sokolov, I. M.: Relative dispersion in fully developed turbulence: the Richardson's law and intermittency correction, Phys. Rev. Lett., 88, 094501, doi:10.1103/PhysRevLett.88.094501, 2002.
Denvich, B. J., Bartello, P., Brenguier, J.-L., Collins, L. R., Grabowski, W. W., Ijzermans, R. H. A., Malinovski, S. P., Reeks, M. W., Vassilicos, J. C., Wang, L.-P., and Warhaft, Z.: Droplet growth in warm turbulent clouds, Q. J. Roy. Meteor. Soc., 138, 1401–1429, 2012.
Gerber, H., Frick, G., Jensen, J. B., and Hudson, J. G.: Entrainment, mixing, and microphysics in trade-wind cumulus, J. Meteorol. Soc. Jpn., 86, 87–106, 2008.
Hill, A. A., Feingold, G., and Jiang, H.: The influence of entrainment and mixing assumption on aerosol–cloud interactions in marine stratocumulus, J. Atmos. Sci., 66, 1450–1464, 2009.
Jeffery, C. A. and Reisner, J. M.: A study of cloud mixing and evolution using PDF methods, Part I: Cloud front propagation and evaporation, J. Atmos. Sci., 63, 2848–2864, 2006.
Khain, A. P., Ovchinnikov, M., Pinsky, M., Pokrovsky, A., and Krugliak, H.: Notes on the state-of-the-art numerical modeling of cloud microphysics, Atmos. Res., 55, 159–224, 2000.
Korolev, A. V.: The influence of suresaturation fluctuations on droplet size spectra formation, J. Atmos. Sci., 52, 3620–3634, 1995.
Korolev, A. and Mazin, I.: Supersaturation of water vapor in clouds, J. Atmos. Sci., 60, 2957–2974, 2003.
Korolev, A., Khain, A., Pinsky, M., and French, J.: Theoretical study of mixing in liquid clouds – Part 1: Classical concept, Atmos. Chem. Phys. Discuss., 15, 30211–30267, doi:10.5194/acpd-15-30211-2015, 2015.
Kovetz, A. and Olund, B.: The effect of coalescence and condensation on rain formation in a cloud of finite vertical extent, J. Atmos. Sci., 26, 1060–1065, 1969.
Krueger, S., Su, C.-W., and McMurtry, P.: Modeling entrainment and finescale mixing in cumulus clouds, J. Atmos. Sci., 54, 2697–2712, 1997.
Kumar, B., Janetzko, F., Schumacher, J., and Shaw, R. A.: Extreme responses of a coupled scalar-particle system during turbulent mixing, New J. Phys., 14, 115020, doi:10.1088/1367-2630/14/11/115020, 2012.
Latham, J. and Reed, R. L.: Laboratory studies of effects of mixing on evolution of cloud droplet spectra, Q. J. Roy. Meteor. Soc., 103, 297–306, 1977.

ACPD
15, 30321–30381, 2015

Lehmann, K., Siebert, H., and Shaw, R. A.: Homogeneous and inhomogeneous mixing in cumulus clouds: dependence on local turbulence structure, J. Atmos. Sci., 66, 3641–3659, 2009.
Magaritz-Ronen, L., Pinsky, M., and Khain, A.: The effective radius vertical profile in stratocumulus clouds, J. Atmos. Sci., in revision, 2015.
Martin, G. M., Johnson, D. W., and Spice, A.: The measurements and parameterization of effective radius of droplets in warm stratocumulus clouds, J. Atmos. Sci., 51, 1823–1842, 1994.
Monin, A. S. and Yaglom, A. M.: Statistical Fluid Mechanics: Mechanics of Turbulence, vol. 2, MIT Press, 1975
Morrison, H. and Grabowski, W. W.: Modeling supersaturation and subgrid-scale mixing with two-moment bulk warm microphysics, J. Atmos. Sci., 65, 792–812, 2008.
Pinsky, M. and Khain, A. P.: Effects of in-cloud nucleation and turbulence on droplet spectrum formation in cumulus clouds, Q. J. Roy. Meteor. Soc., 128, 1–33, 2002.
Pinsky, M., Mazin, I. P., Korolev, A., and Khain, A.: Supersaturation and diffusional droplet growth in liquid clouds, J. Atmos. Sci., 70, 2778–2793, 2013.
Pinsky, M., Mazin, I. P., A. Korolev and Khain, A.: Supersaturation and diffusional droplet growth in liquid clouds: polydisperse spectra, J. Geophys. Res.-Atmos., 119, 12872–12887, 2014.
Pinsky, M., Khain, A., Korolev, A., and Magaritz-Ronen, L.: Theoretical investigation of mixing in warm clouds – Part 2: Homogeneous mixing, 15, 30269–30320, doi:10.5194/acpd-15-30269-2015, 2015.
Polyanin, A. D. and Zaitsev, V. F.: Handbook of Nonlinear Partial Differential Equations, Chapman & Hall/CRC, 809 pp., 2004
Prabha, V. T., Patade, S., Pandithurai, G., Khain, A., Axisa, D., Pradeep Kumar, P., Maheshkumar, R. S., Kulkarni, J. R., and Goswami, B. N.: Spectral width of premonsoon and monsoon clouds over Indo-Gangetic valley during CAIPEEX, J. Geophys. Res., 117, D20205, doi:10.1029/2011JD016837, 2012.
Pruppacher, H. R. and Klett, J. D.: Microphysics of Clouds and Precipitation, 2nd edn., Oxford Press, 914 p., 1997
Rogers, R. R. and Yau, M. K: A Short Course in Cloud Physics, Pergamon Press, 293 pp., 1989
Schlüter M. H.: The Effects of Entrainment and Mixing Process on the Droplet Size Distribution in Cumuli, a thesis submitted to the faculty of The University of Utah in partial fulfillment

ACPD
15, 30321–30381, 2015

of the requirements for the degree of Master of Science, Department of Meteorology, The University of Utah, 92 pp., 2006

Su, C.-W., Krueger, S. K., P. A. McMurtry and Austin, P. H.: Linear eddy modeling of droplet spectral evolution during entrainment and mixing in cumulus clouds, Atmos. Res., 47–48, 41–58, 1998.

Telford, J. W. and Chai, S. K.: A new aspect of condensation theory, PageOph 118, 720–742, 1980.

Warner, J.: The microstructure of cumulus cloud, Pt. I, general features of the droplet spectrum, J. Atmos. Sci., 26, 1049–1059, 1969.

Warner, J.: The microstructure of cumulus cloud: Part 4: The effect on the droplet spectrum of mixing between cloud and environment, J. Atmos. Sci., 30, 256–261, 1973.

ACPD

15, 30321–30381, 2015

Table 1. Different quantities and their non-dimensional forms*.

Quantity	Symbol	Non-dimensional form	Range of normalized values
Time	t	$\widetilde{t} = \frac{t}{\tau_0}$	$[0, \ldots, \infty]$
Distance	x	$\widetilde{x} = \frac{x}{L}$	$[0, \ldots, 1]$
Square of radius	σ	$\widetilde{\sigma} = \frac{\sigma}{r_0^2}$	$[0, \ldots, 1]$
Droplet concentration	N	$\widetilde{N} = \frac{N}{N_1}$	$[0, \ldots, 1]$
LWC	q_w	$\widetilde{q} = \frac{q_\mathrm{w}}{q_{\mathrm{w}1}}$	$[0, \ldots, 1]$
Distribution of square of radius	$f(\sigma)$	$\widetilde{f}(\widetilde{\sigma}) = \frac{r_0^2}{N_1} f(\sigma)$	
Conservative function	Γ	$\widetilde{\Gamma} = \frac{\Gamma}{A_2 q_{\mathrm{w}1}}$	$[-\infty, \ldots, 1]$
Supersaturation	S	$\widetilde{S} = \frac{S}{A_2 q_{\mathrm{w}1}}$	$[-\infty, \ldots, 0]$
Relaxation time	τ_pr	$\widetilde{\tau}_\mathrm{pr} = \frac{\tau_\mathrm{pr}}{\tau_0}$	$[1, \ldots, \infty]$
Damkölher number	Da	$Da = \frac{\tau_\mathrm{mix}}{\tau_0} = \frac{L^2}{K\tau_0}$	$[0, \ldots, \infty]$
Non-dimensional parameter	R	$R = \frac{S_2}{A_2 q_{\mathrm{w}1}}$	$[-\infty, \ldots, 0]$

* All normalizing values depend on initially given values L, N_1, r_0, A_2, S_2, K.

ACPD
15, 30321–30381, 2015

Table 2. Comparison of classical concept and results of the present study.

Classical concept	The present study
The final equilibrium state is typically analyzed; in-situ observations are interpreted assuming the equilibrium state.	The mixing period can last several minutes. The microphysical structure during this period can differ substantially from that at the final stage.
Types of mixing are typically separated into homogeneous and extremely inhomogeneous.	There are the wide ranges of *Da* and *R*, when mixing can be attributed to the intermediate and to inhomogeneous (but not extremely inhomogeneous).
Mixing can start as purely homogeneous.	Any mixing between different volumes starts with the inhomogeneous stage.
Homogeneous mixing leads to a DSD shift to small droplet sizes.	Homogeneous mixing does not always lead to a DSD shift to small droplet sizes (Pt2).
Mixing can be analyzed within the frame of a monodisperse DSD.	Mixing always leads to formation of polydisperse DSD.
In the course of homogeneous mixing, droplet concentration remains constant.	In the course of homogeneous mixing, droplet concentration does not always remain constant (Pt2).
Extremely inhomogeneous mixing does not change the DSD shape.	Inhomogeneous mixing, including extremely inhomogeneous) leads to broadening of DSD towards small sizes.
In the course of inhomogeneous mixing, the effective radius remains constant.	The effective radius varies only slightly (5–20 %) in an initially cloudy volume. The effective radius rapidly increases in an initially non-cloudy volume, approaching the size found in cloudy volumes. With increase in *Da* the difference between values of effective radius in the initially cloud volume and that in the final state decreases in agreement with the classical concept.

ACPD
15, 30321–30381, 2015

Table A1. List of symbols.

Symbol	Description	Units
A_2	$\frac{1}{q_v} + \frac{L_w^2}{c_p R_v T^2}$, coefficient	–
a_0, a_n	Fourier series coefficients	–
C	Richardson's law constant	–
c_p	specific heat capacity of moist air at constant pressure	$\mathrm{J\,kg^{-1}\,K^{-1}}$
D	coefficient of water vapour diffusion in air	$\mathrm{m^2\,s^{-1}}$
Da	Damkölher number	–
e	water vapour pressure	$\mathrm{N\,m^{-2}}$
e_w	saturation vapour pressure above flat surface of water	$\mathrm{N\,m^{-2}}$
F	$\left(\frac{\rho_w L_w^2}{k_a R_v T^2} + \frac{\rho_w R_v T}{e_w(T) D}\right)$, coefficient	$\mathrm{m^{-2}\,s}$
$f(\sigma)$	distribution of square radius	$\mathrm{m^{-5}}$
$\widetilde{f}(\widetilde{\sigma})$	normalized distribution of square radius	–
$g(r)$	droplet size distribution	$\mathrm{m^{-4}}$
k_a	coefficient of air heat conductivity	$\mathrm{J\,m^{-1}\,s^{-1}\,K^{-1}}$
K	turbulent diffusion coefficient	$\mathrm{m^2\,s^{-1}}$
L	characteristic spatial scale of mixing	m
L_w	latent heat for liquid water	$\mathrm{J\,kg^{-1}}$
m_α	moment of DSD of order α	
N	droplet concentration	$\mathrm{m^{-3}}$
$\widetilde{N}$	normalized droplet concentration	–
N_1	initial droplet concentration in cloud volume	$\mathrm{m^{-3}}$
p	pressure of moist air	$\mathrm{N\,m^{-2}}$
q_v	water vapour mixing ratio (mass of water vapour per 1 kg of dry air)	–
q_w	liquid water mixing ratio (mass of liquid water per 1 kg of dry air)	–
q_{w1}	liquid water mixing ratio in cloud volume	–
$\widetilde{q}$	normalised liquid water mixing ratio	–
R	$\frac{S_2}{A_2 q_{w1}}$, non-dimensional parameter	–
R_a	specific gas constant of moist air	$\mathrm{J\,kg^{-1}\,K^{-1}}$
R_v	specific gas constant of water vapour	$\mathrm{J\,kg^{-1}\,K^{-1}}$
r	droplet radius	m
r_0	initial droplet radius	m
$\overline{r}$	mean droplet radius	m
S	$e/e_w - 1$, supersaturation over water	–
$\widetilde{S}$	normalized supersaturation	–
S_2	initial supersaturation in dry volume	–
$\widetilde{S}_{max}$	normalized initial maximal saturation deficit	–
T	temperature	K
T_{mix}	normalized duration of inhomogeneous stage	–
T_{ev}	normalized duration of evaporation	–
T_{tot}	normalized duration of mixing	–
t	time	s
$\widetilde{t}$	non-dimensional time	–
x	distance	m
$\widetilde{x}$	non-dimensional distance	–
λ_1, λ_2	criteria of delimitation between the types of mixing	–
ε	turbulent dissipation rate	$\mathrm{m^2\,s^{-3}}$
$\Gamma(x,t)$	conservative function	–
$\widetilde{\Gamma}$	normalized conservative function	–
ρ_a	density of air	$\mathrm{kg\,m^{-3}}$
ρ_w	density of liquid water	$\mathrm{kg\,m^{-3}}$
σ	square of droplet radius	$\mathrm{m^2}$
$\widetilde{\sigma}$	normalized square of droplet radius	–
τ_{pr}	phase relaxation time	s
$\widetilde{\tau}_{pr}$	normalized phase relaxation time	–
τ_{mix}	characteristic time of mixing	s
τ_0	initial scale	s

ACPD
15, 30321–30381, 2015

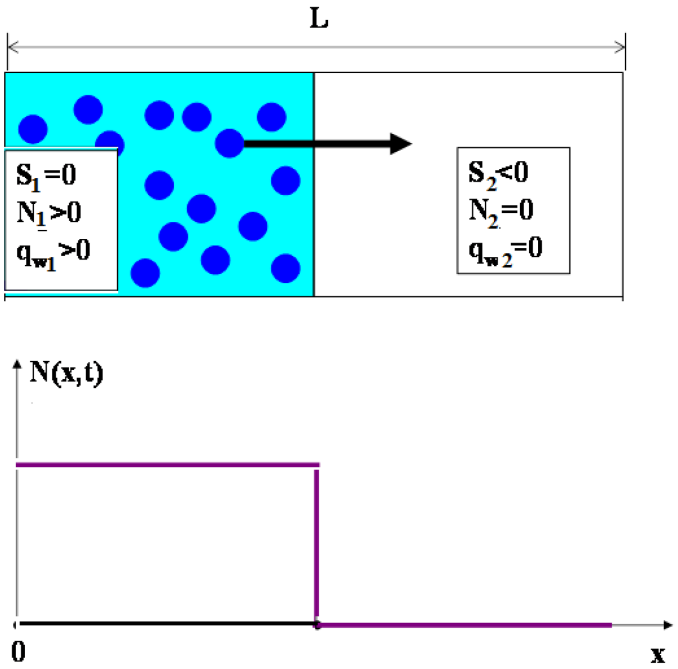

Figure 1. 1-D geometry of the problem considered in the study. The initial state at $t = 0$ is illustrated. The left volume is a saturated cloudy volume; the right volume is a non-saturated air volume from the cloud environment.

ACPD
15, 30321–30381, 2015

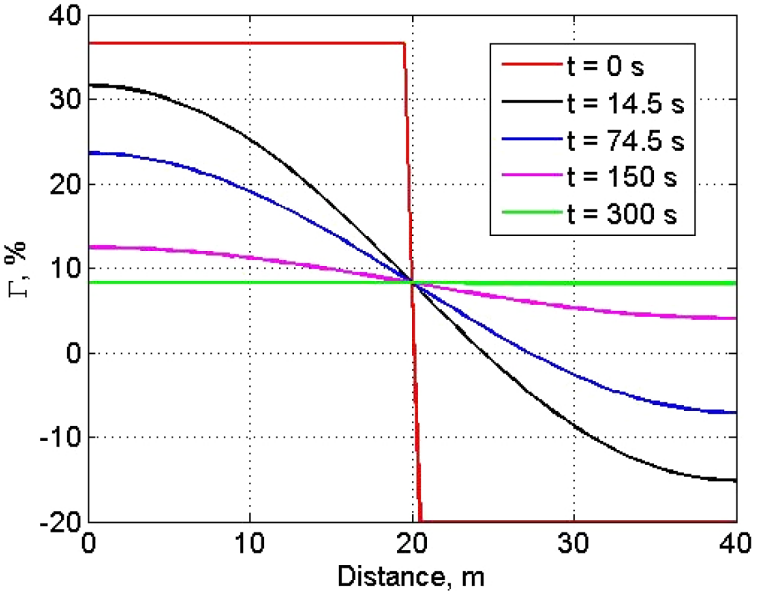

Figure 2. An example of evolution $\Gamma(x,t)$ during mixing.

ACPD
15, 30321–30381, 2015

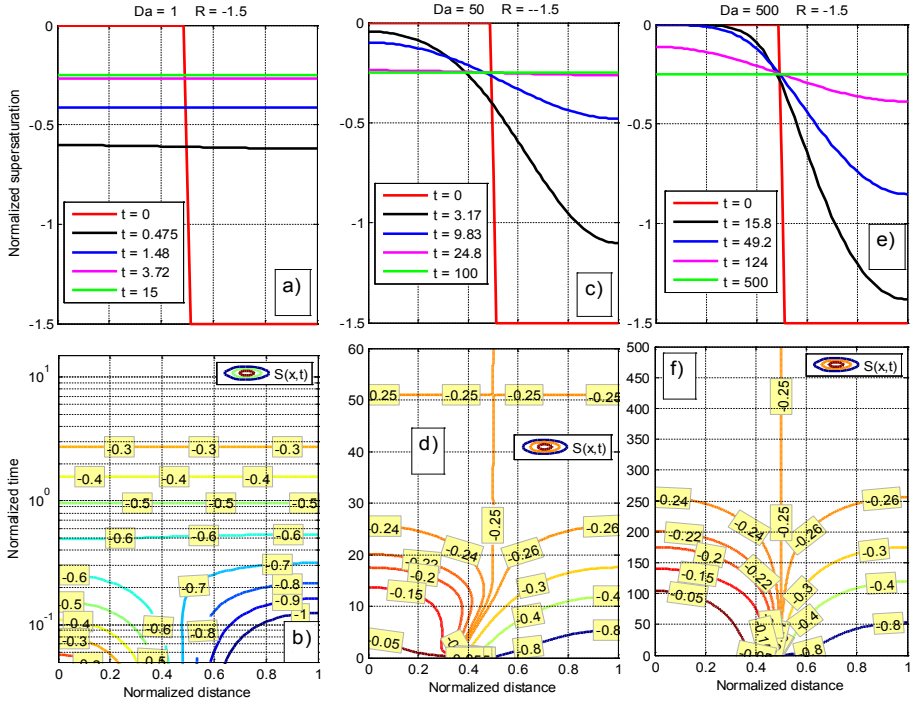

Figure 3. Horizontal dependencies (upper row) and $\widetilde{x} - \widetilde{t}$ dependencies (lower row) of normalized saturation deficit for Da = 1, 50 and 500 and R = −1.5. Panel b is plotted in semi-log scale.

ACPD
15, 30321–30381, 2015

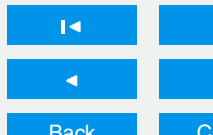

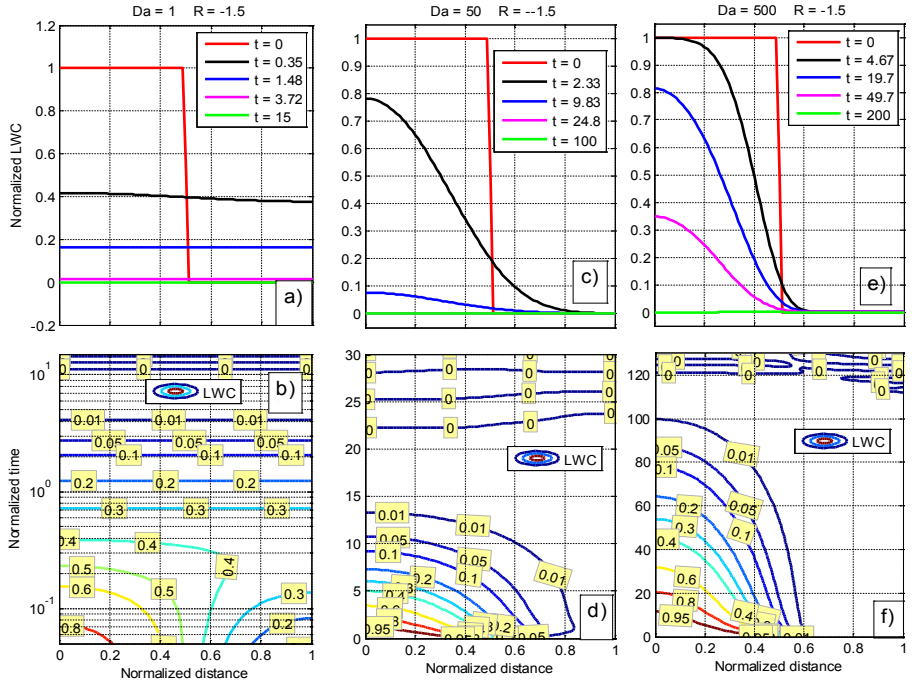

Figure 4. The same as in Fig. 3, but for LWC. Lower-left panel is plotted in semi-log scale.

ACPD
15, 30321–30381, 2015

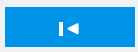

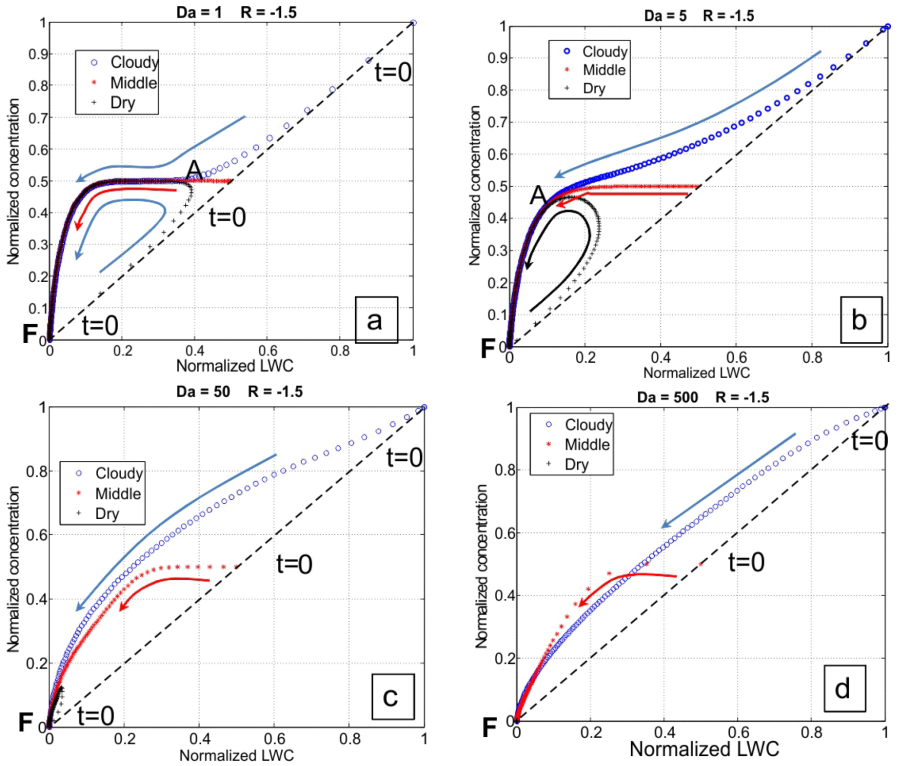

Figure 5. Dependencies between normalized values of droplet concentration and LWC at different *Da* and $R = -1.5$. Blue symbols correspond to the centre of the cloudy volume ($\widetilde{x} = 1/4$), red symbols correspond to the interface between cloudy and dry volumes ($\widetilde{x} = 1/2$) and black crosses correspond to $\widetilde{x} = 3/4$, i.e. the centre of the initially dry volume. Symbols at $t = 0$ show initial states at these three values of $\widetilde{x}$. Arrows show direction of movement of the points at the diagram with time. Letter "A" corresponds to the beginning of spatially homogeneous stage, $\widetilde{t} = T_{\mathrm{mix}}$. Letter "F" corresponds to the final state. The dashed line indicates relationship between $\widetilde{N}$ and $\widetilde{q}$ for extremely inhomogeneous mixing according to classical concept.

ACPD
15, 30321–30381, 2015

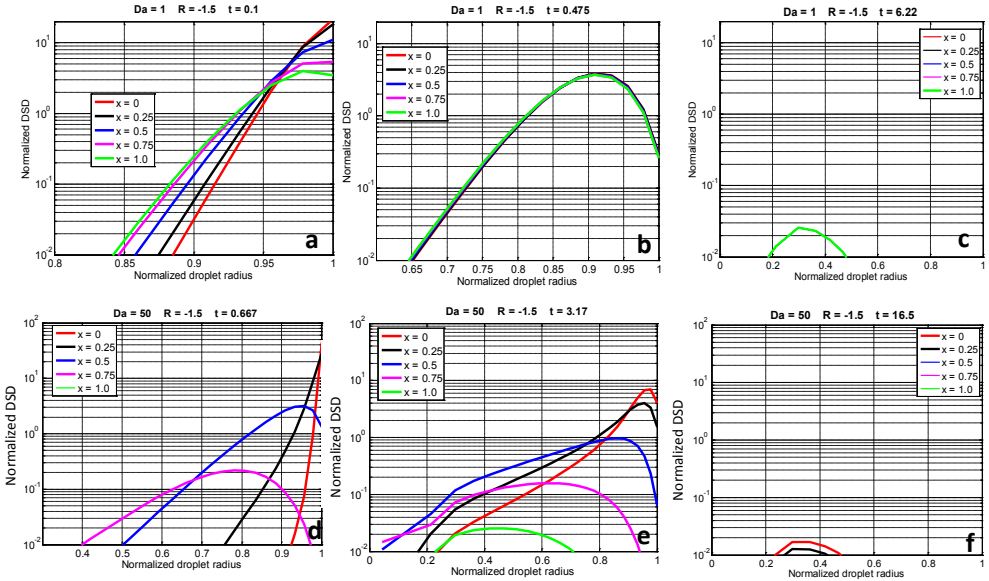

Figure 6. Time evolution of DSD during droplet evaporation at $Da = 1$ (upper row) and $Da = 50$ (bottom row). At each panel, the normalized DSD are shown at different values of horizontal coordinate $\widetilde{x}$. Different panels show DSDs at different time instances.

ACPD
15, 30321–30381, 2015

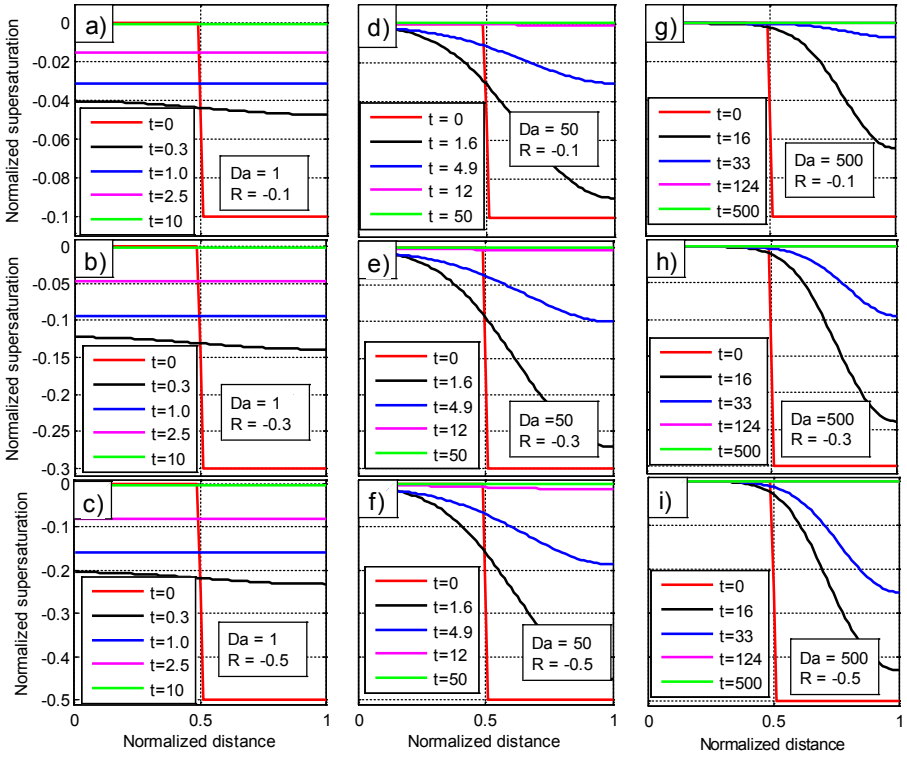

Figure 7. Profiles of normalized supersaturation at different *Da* and *R*.

ACPD
15, 30321–30381, 2015

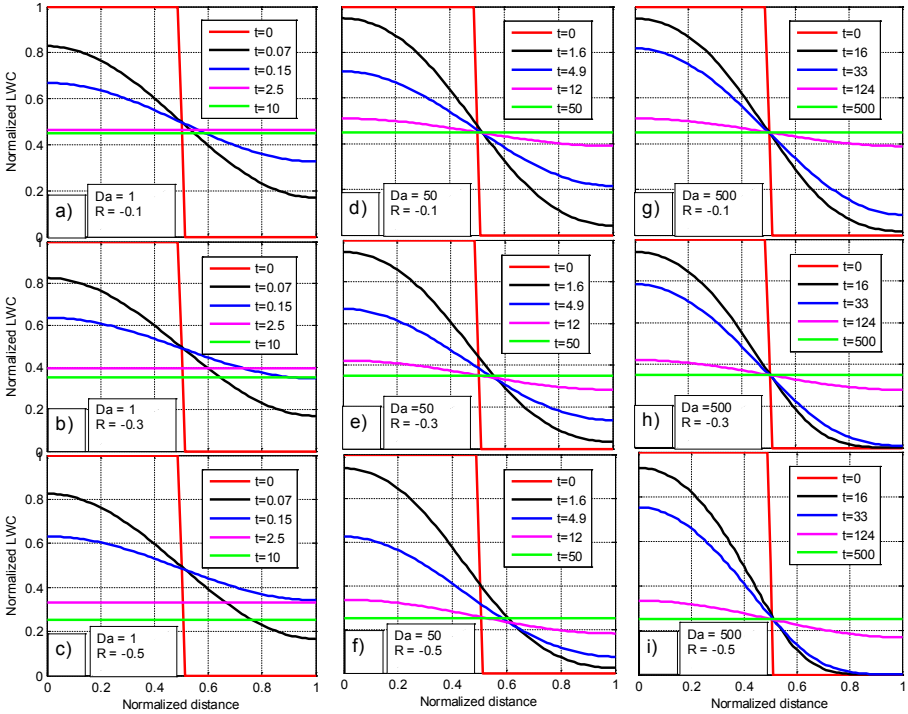

Figure 8. Profiles of normalized LWC at different *Da* and $R > -1$.

ACPD
15, 30321–30381, 2015

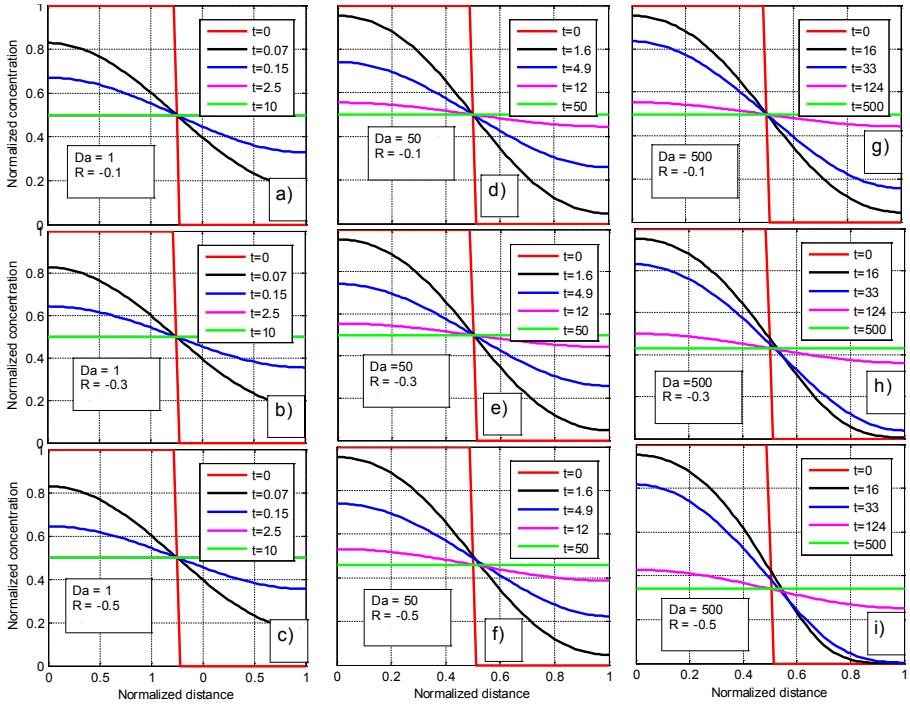

Figure 9. Profiles of normalized droplet concentration at different *Da* and *R*.

ACPD
15, 30321–30381, 2015

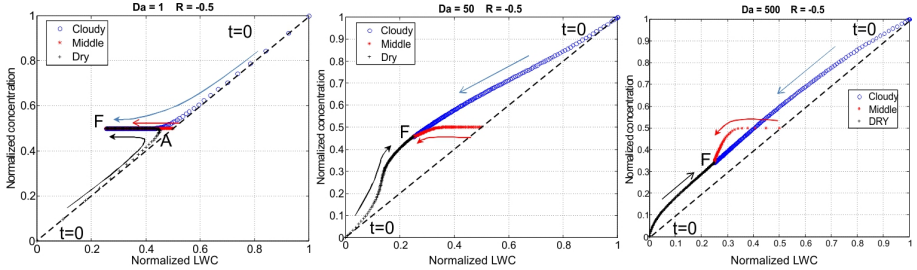

Figure 10. Dependencies between normalized values of droplet concentration and LWC at different *Da* and $R = -0.5$. Blue circles denote the centre of the cloudy volume ($\widetilde{x} = 1/4$), red symbols denote the initial interface ($\widetilde{x} = 1/2$) and black crosses correspond to $\widetilde{x} = 3/4$, the centre of the initially dry volume. Arrows show the direction of movement of the points at the diagram with time. Point "F" denotes the final stationary state of the system. The dashed line indicates relationship between $\widetilde{N}$ and $\widetilde{q}$ for extremely inhomogeneous mixing according to the classical concept (Pt1).

ACPD
15, 30321–30381, 2015

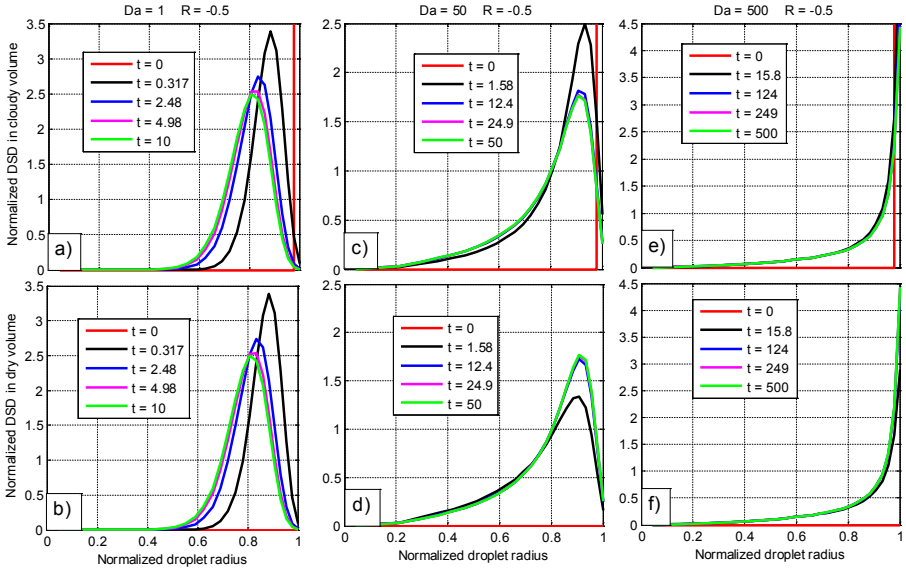

Figure 11. Examples of DSD evolution in initially an cloudy volume ($\widetilde{x} = 1/4$) (upper row) and in an initially dry volume ($\widetilde{x} = 3/4$) (lower row) at $R = -0.5$ and different values of *Da*.

ACPD
15, 30321–30381, 2015

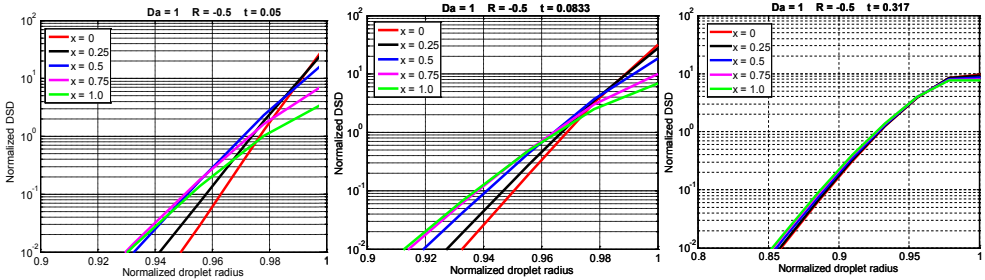

Figure 12. DSDs at different $\widetilde{x}$ at the beginning of the mixing process for $Da = 1$ and $R = -0.5$.

ACPD
15, 30321–30381, 2015

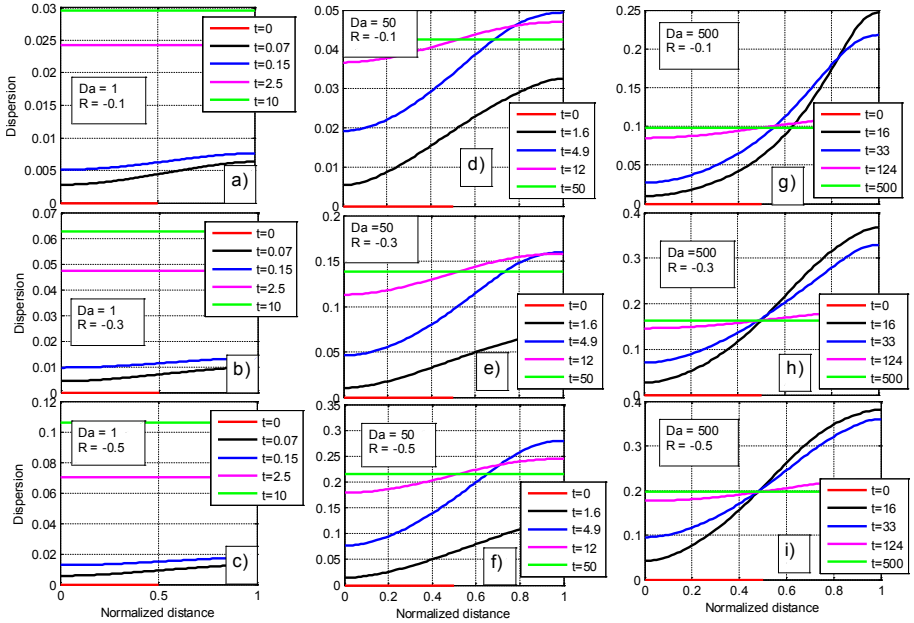

Figure 13. Spatial dependencies of relative DSD dispersion at different time instances, and values of *Da* and *R*.

ACPD
15, 30321–30381, 2015

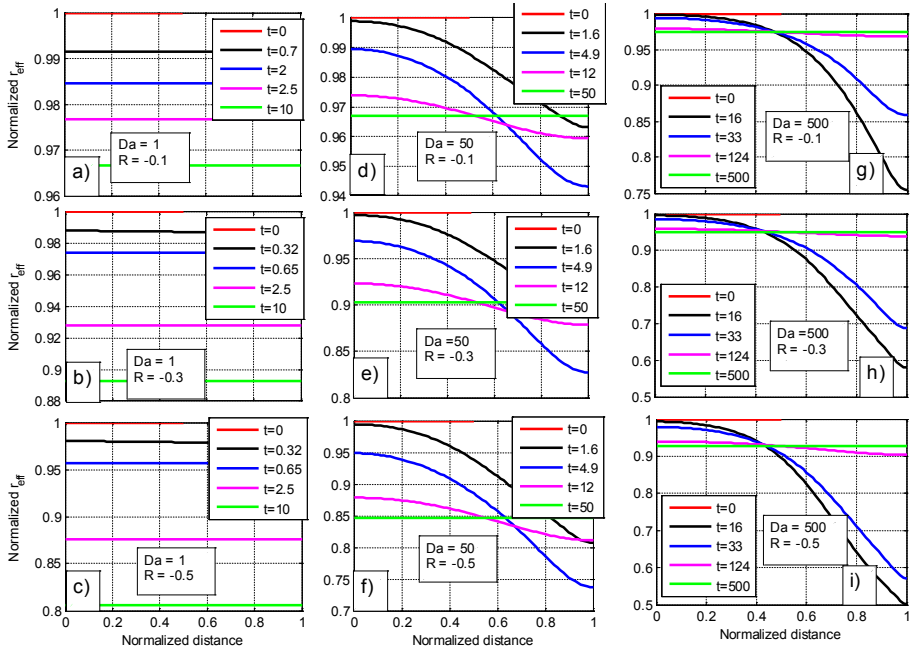

Figure 14. Spatial dependencies of effective radius at different time instances, and values of *Da* and *R*.

ACPD
15, 30321–30381, 2015

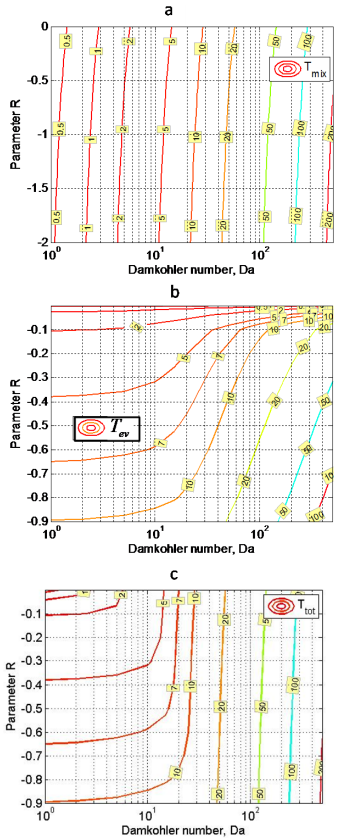

Figure 15. Contours of normalized mixing duration times on Da–R plane. **(a)** Mixing time, T_{mix}, **(b)** evaporation time, T_{ev}, and **(c)** total duration mixing time T_{tot}.

ACPD
15, 30321–30381, 2015

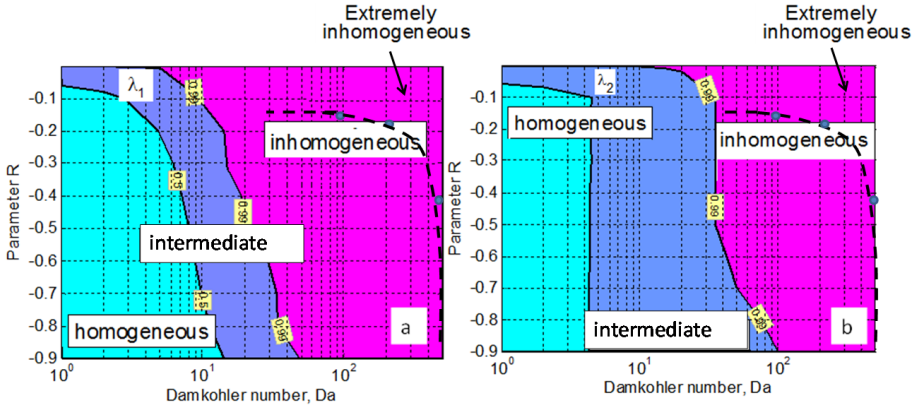

Figure 16. (a) The boundaries between types of mixing on the *Da*–*R* plane designed according to criteria $\lambda_1 = \frac{T_{mix}}{T_{tot}}$; **(b)** the boundaries between types of mixing on the *Da*–*R* plane designed according to criterion $\lambda_2 = \frac{2\langle\tilde{q}(T_{mix})\rangle - 1}{R}$ (Eq. 41). Dashed lines indicate the line corresponding to 2 % deviation from initial mean volume radius.

ACPD
15, 30321–30381, 2015

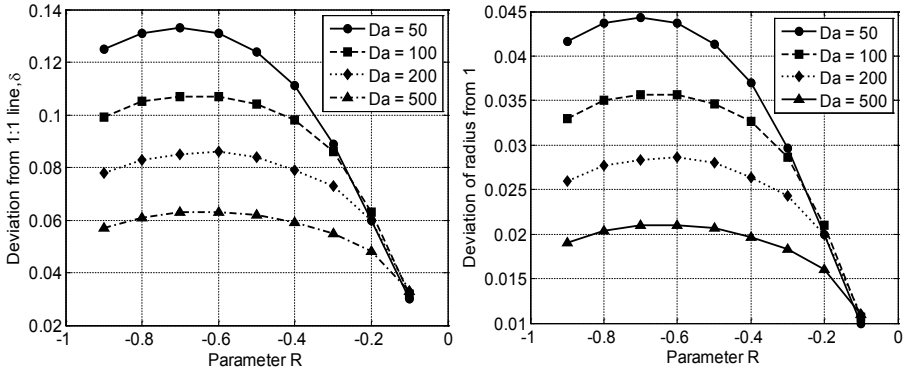

Figure 17. Left: Dependencies of the r.m.s. distance of the $\widetilde{N}$–$\widetilde{q}$ relationships from straight line 1 : 1 suggested by classical concept of extremely inhomogeneous mixing. The dependencies are plotted for different values of *Da* and *R*. Right: The same as to left but for r.m.s. deviations of mean volume radius from initial constant value suggested by the classical concept.

ACPD
15, 30321–30381, 2015